Article

Cell Reports

Disentangling Pro-mitotic Signaling during Cell Cycle Progression using Time-Resolved Single-Cell Imaging

Graphical Abstract

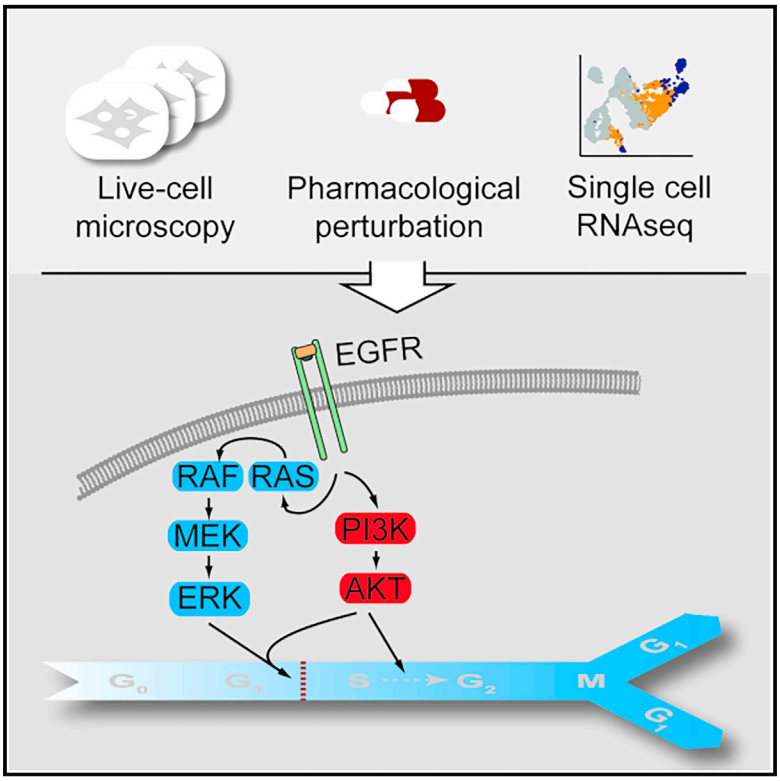

Authors

Manuela Benary, Stefan Bohn, Mareen Lüthen, Ilias K. Nolis, Nils Blüthgen, Alexander Loewer

Correspondence

nils.bluethgen@charite.de (N.B.), loewer@bio.tu-darmstadt.de (A.L.)

In Brief

Combining quantitative live-cell microscopy and single-cell sequencing with pharmacological perturbation, Benary et al. disentangle the dynamic requirements of EGF-induced MAPK and PI3K activity during mitogenic signaling. They corroborate that both pathways are necessary to induce S-phase entry and show that only PI3K is needed to drive replication by metabolic adjustments.

Highlights

- The contribution of EGF-induced signaling pathways is decomposed in single cells
- Critical dynamic features are identified by information theory
- ERK and PI3K activity are necessary for initial cell cycle entry
- PI3K is necessary later to adjust the metabolism of the cell during replication

Benary et al., 2020, Cell Reports *31*, 107514
April 14, 2020
https://doi.org/10.1016/j.celrep.2020.03.078

CellPress

Cell Reports
Article

Disentangling Pro-mitotic Signaling during Cell Cycle Progression using Time-Resolved Single-Cell Imaging

Manuela Benary,[1,2,3,7] Stefan Bohn,[4,7] Mareen Lüthen,[1,5] Ilias K. Nolis,[6] Nils Blüthgen,[1,2,3,5,*] and Alexander Loewer[4,6,8,*]
[1]Institute of Pathology, Charité-Universitätsmedizin Berlin, 10117 Berlin, Germany
[2]Institute for Theoretical Biology, Charité-Universitätsmedizin Berlin, 10115 Berlin, Germany
[3]Integrative Research Institute Life Sciences, Humboldt University Berlin, 10115 Berlin, Germany
[4]Department of Biology, Technische Universität Darmstadt, 64287 Darmstadt, Germany
[5]German Cancer Consortium (DKTK), German Cancer Research Center (DKFZ), 69120 Heidelberg, Germany
[6]Berlin Institute for Medical Systems Biology, Max Delbrueck Center in the Helmholtz Association, 13125 Berlin, Germany
[7]These authors contributed equally
[8]Lead Contact
*Correspondence: nils.bluethgen@charite.de (N.B.), loewer@bio.tu-darmstadt.de (A.L.)
https://doi.org/10.1016/j.celrep.2020.03.078

SUMMARY

Cells rely on input from extracellular growth factors to control their proliferation during development and adult homeostasis. Such mitogenic inputs are transmitted through multiple signaling pathways that synergize to precisely regulate cell cycle entry and progression. Although the architecture of these signaling networks has been characterized in molecular detail, their relative contribution, especially at later cell cycle stages, remains largely unexplored. By combining quantitative time-resolved measurements of fluorescent reporters in untransformed human cells with targeted pharmacological inhibitors and statistical analysis, we quantify epidermal growth factor (EGF)-induced signal processing in individual cells over time and dissect the dynamic contribution of downstream pathways. We define signaling features that encode information about extracellular ligand concentrations and critical time windows for inducing cell cycle transitions. We show that both extracellular signal-regulated kinase (ERK) and phosphatidylinositol 3-kinase (PI3K) activity are necessary for initial cell cycle entry, whereas only PI3K affects the duration of S phase at later stages of mitogenic signaling.

INTRODUCTION

Mammalian cells harbor complex, interlinked signal transduction networks that relay information from the outside of the cell to the inside. These networks allow cells to sense fine-grained information about their environment and control cellular physiology by regulating gene expression or influencing processes like cytoskeletal organization. However, they are also subject to molecular noise from cell-intrinsic sources, such as fluctuations in the levels of signaling proteins, and external influences, such as changes in their local environment (Snijder and Pelkmans, 2011). Although we have gained a good understanding of the molecular foundation of cellular signaling, we are still challenged to understand how signaling pathways interact dynamically to mediate reliable cell fate decisions despite the variable conditions present in individual cells.

Among the most important cellular decisions is the control of proliferation. In a multicellular organism, the rate and timing of cell division need to be precisely coordinated to allow growth during development and tissue homeostasis during adult life. Cells, therefore, rely on mitogenic stimuli, such as epidermal growth factor (EGF) and their respective receptors, to initiate cell cycle entry. A crucial mediator of mitogenic signals is the mitogen-activated protein kinase (MAPK) pathway (Seger and Krebs, 1995; Figure 1A): activation of the EGF receptor (EGFR) and the small GTPase RAS induces phosphorylation and activation of the kinases rapidly accelerated fibrosarcoma (RAF), MAPK/ERK kinase (MEK), and extracellular signal-regulated kinase (ERK). Upon phosphorylation, ERK translocates to the nucleus and activates transcription of target genes. Among the first target genes expressed is the transcription factor FOS. In addition to activating its mRNA expression, ERK phosphorylates and stabilizes the FOS protein. Therefore, target genes of FOS, such as FRA1/FOSL1, which is also stabilized by ERK phosphorylation, will be induced only by prolonged activity of ERK (Marshall, 1995). In addition to this temporal encoding, information in the MAPK pathway may be encoded by the amplitude and duration of the signal (Heinrich et al., 2002) or other features like frequency and amplitude of oscillation in the localization of ERK (Shankaran et al., 2009). ERK promotes proliferation by inducing expression of Cyclin D and repression of cyclin-dependent kinase (CDK) inhibitors (Rubinfeld and Seger, 2005; Zhang and Liu, 2002). Upon activation, CDKs phosphorylate the retinoblastoma protein and release E2F transcription factors, which regulate complex changes in cellular physiology that mark the transition from G1 to S phase of the cell cycle (Harbour and Dean, 2000; Yao et al., 2008). Other signaling-induced processes, such as expression and stabilization of c-*myc*, contribute to regulating the G1 to S phase transition (Leung et al., 2008).

In addition to the MAPK pathway, EGFR also activates the PI3K/AKT pathway through direct or indirect recruitment and activation of the p85/p110 kinase complex. PI3K activity leads

to the generation of phosphatidylinositol-3,4,5-triphosphate, which in turn recruits the kinase AKT to the membrane, where it is activated by PDK1. Through activation of mechanistic target of rapamycin kinase (mTOR), AKT influences translation and contributes to Cyclin D accumulation during cell cycle entry (Hay and Sonenberg, 2004). In addition, AKT also mediates inhibitory phosphorylation of the Cyclin D repressor FOXO (Schmidt et al., 2002) and the kinase GSK3beta, which induces Cyclin D degradation (Dong et al., 2005). Furthermore, AKT signaling may contribute to other cell cycle transitions by affecting the activity and localization of regulatory proteins and controlling metabolism (Ward and Thompson, 2012). The PI3K and MAPK pathways interact closely upon mitogenic stimulation (Chen et al., 2012; Moelling et al., 2002). It has been suggested that both pathways are compensatory through co-regulated proteins (Zwang et al., 2011). Other reports indicate that AKT negatively regulates MAPK activity through inactivation of RAF (Zimmermann and Moelling, 1999), whereas MEK suppresses PI3K signaling by promoting membrane localization of the phosphatase PTEN (Zmajkovicova et al., 2013).

In summary, the importance and synergy of ERK and AKT in initiating the cell cycle from G0 to S phase has been well researched, such as the mechanisms by which these pathways interact in controlling Cyclin D. In contrast, the relative roles of AKT and ERK in controlling later stages are less clear. We, therefore, set out to investigate the temporal role of ERK and its relative importance to other pathways in cell cycle control throughout the cell cycle. To this end, we quantified EGF-induced mitogenic signaling and deconvolved the dynamic contributions of downstream signaling pathways by combining time-resolved single-cell measurements of ERK activity and cell cycle progression in an untransformed human cell line with targeted pharmacological perturbations and statistical analysis. Using this approach, we define features of ERK activity that encode information about extracellular ligand concentration and determine the time window where it is necessary for cell cycle entry. We show that both ERK and PI3K activity are necessary for initial cell cycle entry, whereas only PI3K affects the duration of S phase at later stages of the mitogenic signaling.

RESULTS

Quantitative Live-Cell Imaging Reveals Cell-Specific Activation Patterns of the EGFR/ERK Pathway

To analyze EGF-induced signaling in living cells on physiologically relevant timescales, we used a previously established MCF10A reporter cell line. This reporter termed FIRE is based on the fluorescent protein mVenus fused to a nuclear localization signal and the PEST domain of FRA1, a transcription factor stabilized by ERK phosphorylation (Albeck et al., 2013; Figures 1A and S1A). In the absence of mitogenic stimuli activating the EGFR/ERK pathway, the constitutively expressed reporter is rapidly degraded. When cells are treated with EGF, FIRE is stabilized through ERK-dependent phosphorylation and accumulates in the nucleus (Figure 1B). It, therefore, provides a specific linear measure of the integrated activity of the EGFR/ERK pathway over long, physiologically relevant timescales (Gillies et al., 2017), which we verified using small-molecule inhibitors (Figures S1B and S1C).

As we were mainly interested in following mitogenic signaling during the progression of quiescent cells from the G0 phase of the cell cycle to mitosis, we withdrew mitogenic growth factors and serum for 48 h before stimulating reporter cells with defined EGF doses spanning two orders of magnitude from 0.5 ng/ml to 50 ng/ml. We then measured the nuclear fluorescence intensity of FIRE for 48 h and generated time-resolved trajectories of FIRE intensity, representing more than 850 individual cells per condition by using automated image analysis followed by data processing and normalization (Figures S1D and S1E; STAR Methods; Table S1). Without EGF, cells showed no detectable changes in reporter activity, indicating that there was no residual input to the MAPK pathway under our experimental conditions (Figures 1B and 1C). At low EGF concentrations, we observed transient FIRE accumulation during the first 10–15 h, with homogeneous timing and amplitude. When stimulated with EGF concentrations above 2.5 ng/ml, cells showed a second phase of FIRE activity after about 15 h. This pattern of pathway activity was also reflected in the mean response of all cells treated with a given dose of EGF, which showed a first phase of reporter activity at about 10 h for all conditions and a second phase of increasing amplitude and duration for EGF concentrations above 2.5 ng/ml (Figure 1D). Our observations are consistent with feedback regulation of the ERK pathway and EGF degradation, which is exponential with a half-life of about 10 h for low EGF concentration (Figure S1F). In contrast, EGF decays sub-exponentially and remains elevated during the observed time period for higher EGF concentrations, inducing the second signaling phase. On the single-cell level, most cells showed a first FIRE response at EGF concentrations as low as 1 ng/ml, whereas the fraction of cells showing a second phase of FIRE signals saturated at EGF concentrations of 5 ng/ml or higher (Figure 1E).

The Strength of Mitogenic Signaling Is Encoded by Dynamic Features of Integrated ERK Activity

To better understand how individual cells encode the strength of mitogenic stimuli, we defined characteristic features of FIRE dynamics and used information theory to determine the extent to which they carry information about extracellular EGF concentrations. Using the mean responses to different EGF concentrations as guides, we focused on the amplitude, fold change, timing of the maximum, duration and area under the curve of the FIRE signal separately for up to 15 h (first phase) as well as for the remaining time course after 20 h (second phase, Figure 2A). We used mutual information as a measure of the interdependence between these features and EGF concentration. More precisely, we calculated mutual information between EGF concentrations and individual as well as all pairwise combinations of these features. Mutual information quantifies how much information one variable conveys about the other variable. Therefore, it allows us to quantify how much information about the extracellular EGF concentration can be inferred from different features of the FIRE response. We observed that the logarithmic fold change during the first and second signaling phase was the combination with the highest mutual information, resulting in a value of about 1.4 bits (Figure 2B). Mutual information of 1.4 bits indicates that it is possible to infer approximately three levels of EGF

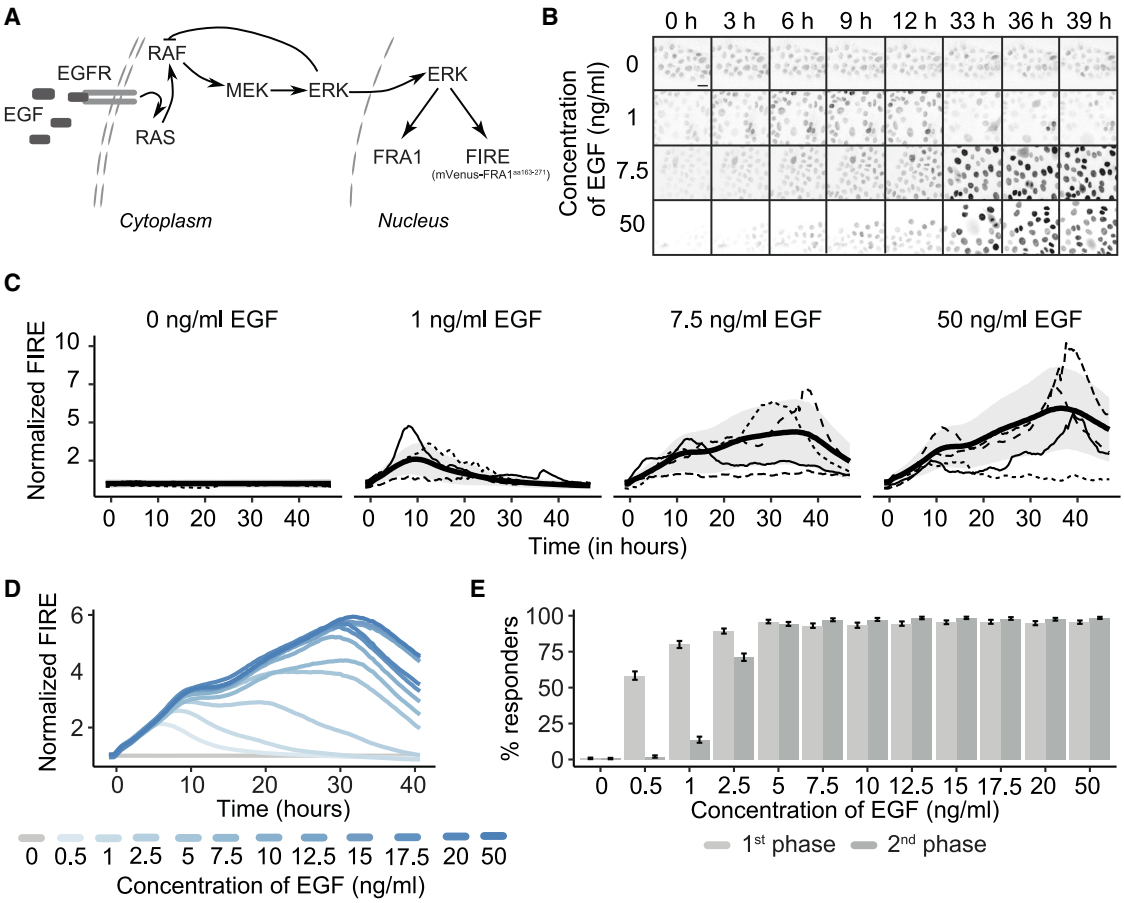

Figure 1. ERK Activity in Living Cells

(A) Scheme of the EGF pathway, where EGFR stimulation triggers the activation of RAF, MEK, and ERK by phosphorylation. ERK translocates to the nucleus, where it phosphorylates numerous targets, including the transcription factor FRA1. Phosphorylation of the PEST domain of FRA1 by ERK leads to stabilization of the protein. We used a fluorescent reporter that contains the PEST domain of FRA1 and is stabilized by ERK phosphorylation (FIRE). See also Albeck et al. (2013).

(B) Example images of the FIRE reporter at indicated time points and EGF concentrations. Scale bar: 24 μm.

(C) Examples of single-cell FIRE reporter time series for randomly selected single cells treated with indicated EGF concentrations. Mean time courses (bold lines) and standard deviations (gray ribbons) of all measured cells are indicated. Growth factor and serum-deprived cells were treated with the indicated doses of EGF. Images were acquired every 20 min for 46 h.

(D) Average FIRE reporter time series for concentrations from 0 ng/ml EGF to 50 ng/ml EGF. Color indicates EGF concentration.

(E) Percentage of cells showing a response within 16 h (light gray) after stimulation and between 20 h after stimulation and the end of measurement (gray). Cells with amplitudes greater than three standard deviations from the average of unstimulated cells were considered to be responding. Error bars indicate 95% confidence interval based on bootstrapping (n = 1,000).

See also Figure S1.

stimulation from the FIRE response. When inspecting the distributions of these features for different EGF concentrations (Figures 2C and S2A), we noticed that both were very low for most untreated cells, whereas stimulation with EGF resulted in logarithmic fold changes of about 1.5 at early time points in most cells. The logarithmic fold change for the second phase was clearly different between low and high doses of EGF (Figures 2C and S2B), as stimulation with, for example, 1 ng/ml resulted in fold changes below 1 in most cases, whereas stimulation above 7.5 ng/ml resulted in much higher logarithmic fold changes of 2–3. Therefore, the fold change of the first phase allowed us to discriminate if the cells were stimulated and the fold change of the second phase allowed us to discriminate between high and low dose (Figure 2D). When considering both first and second phase, the response to three different concentrations of EGF can be well separated (Figure 2D).

To determine if our focus on selected features of the dynamic response restricted the information theoretical analysis of EGF signaling, we clustered entire time series based on Euclidean distance using the k-means algorithm (Figures S3A and S3B; STAR Methods). However, mutual information calculated for EGF concentrations and clusters of time series saturated at about 1 bit, well below the 1.4 bits calculated for the most informative combination of features (Figure S3C). The information content of individual time points of the FIRE measurements as well as of immunofluorescent measurements of selected

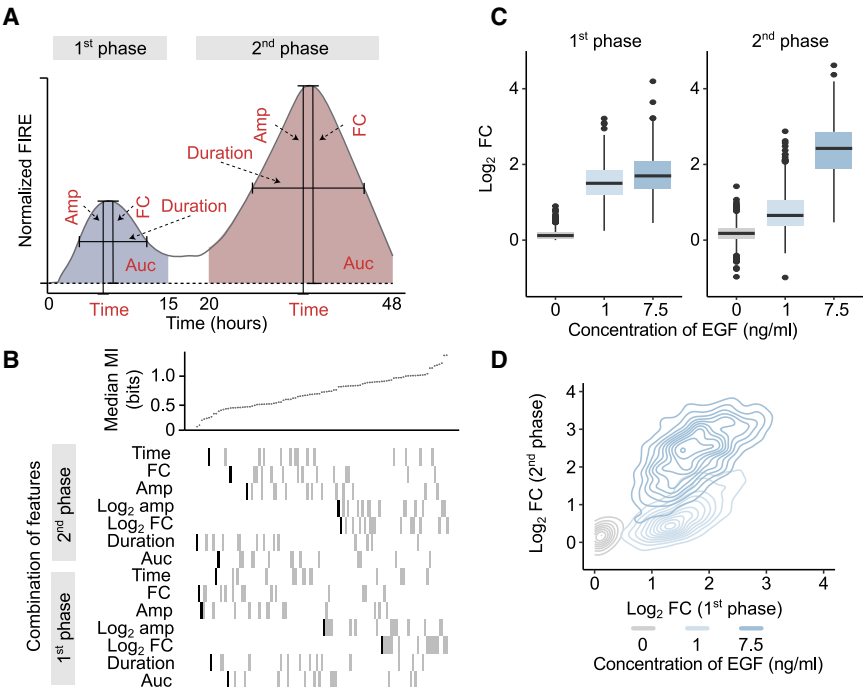

Figure 2. Bi-phasic ERK Activity Profiles Encode External Ligand Concentration

(A) Scheme of features describing the FIRE response after EGF treatment. The FIRE response is separated into early and late responses, and each phase is characterized by the following features: amplitude (Amp), time of the maximum (Time), fold change of the amplitude (FC), duration of the response, and area under the curve (Auc), as well as log_2-scaled Amp and FC.

(B) Multivariate mutual information (top panel) between EGF concentrations and FIRE features (bottom panel, black: single features, gray: pairwise combinations). Features are sorted by their median mutual information (top panel).

(C) Log_2 FC of the amplitude for the first (left panel) and second response (right panel) for indicated EGF concentrations. Black lines indicate medians of distributions; boxes include data between the 25th and 75th percentiles; whiskers extend to the maximum values within 1.5 × the interquartile range; dots represent outliers.

(D) Contour plot of log_2 FC for the first and second response for indicated concentrations of EGF.

See also Figures S2 and S3.

signaling-induced protein modifications at various time points during the response was even more limited (Figures S3D–S3F).

Therefore, information-theoretical analysis is an elegant tool to assess which features represent the input stimulus most precisely. It suggests that three concentrations of EGF are sufficient to sample and characterize the signaling response in these cells.

ERK Activity Is Necessary but Not Sufficient for Cell Cycle Entry and Progression

After identifying relevant dynamic features of integrated ERK activity, we next aimed to characterize how EGF signaling controls the phenotypic response of individual cells. To this end, we determined if and when cells entered S phase by using a fusion of the red fluorescent protein mCherry (RFP) with the first 110 amino acids of geminin (Albeck et al., 2013; Figure S4A). As geminin is degraded by APC^{Cdh1} during G1 and only accumulates during S and G2 phases (Clijsters et al., 2013; Sakaue-Sawano et al., 2008), we defined an increase of more than 2 × the standard deviation of the basal RFP level as the time of S-phase entry (Figure S4B). This method to determine S-phase entry correlated well with measurements of actively replicating cells marked by 5-ethynyl-2′-deoxyuridine (EdU) incorporation, even at low stimulation levels (Figures S4F–S4H). At the transition between metaphase and anaphase of mitosis, geminin is degraded by APC^{Cdc20}, which led to a sharp decline in the intensity of the geminin reporter (Figure S4B). As the duration of mitosis, in general, and of anaphase and telophase, specifically, is relatively short given the duration of our observation period and the temporal resolution of our experiments, we will refer to the duration of geminin accumulation as the duration of S/G2 phase. Moreover, the beginning of geminin accumulation will be termed S-phase entry and the timing of the metaphase-to-anaphase transition will be termed cell division.

Without EGF stimulation, cells showed neither S-phase entry nor cell division, emphasizing that there was no residual mitogenic activity under our experimental conditions and that all observed cell cycle progression was dependent on EGF-induced signaling. We found more and more cells entering S phase when we increased the stimulus, reaching a maximum of about 90% of the cells at concentrations of 7.5–10 ng/ml EGF (Figure 3A). We observed a similar increase of cells dividing at least once within 48 h, although the fraction of dividing cells remained noticeably lower at around 70% (Figure 3A) as the duration of S/G2 phase extended beyond the observation period in cells with late S-phase entry. Accordingly, the time of S-phase entry was heterogeneously distributed around 20 h post-stimulation in individual cells, mostly independent of the strength of the mitogenic stimulus (Figures 3B and S4C–S4E). A noticeable exception were those cells that responded to very low EGF concentrations, as they only entered S phase at earlier time points, which is consistent with a lack of signal at later times due to rapid decay of EGF under these conditions. The duration of S/G2 phases was similarly distributed with a median around 18 h (Figure 3C). Interestingly, there was no clear correlation between time of S-phase entry and duration of S/G2 phase (Figure 3D).

At low EGF concentrations, only about half of the cells entered S phase (Figure 3A). Therefore, we asked if cells that entered S phase differed in their integrated ERK activity profile, and thus different signaling pathway engagement could be the reason for the heterogeneity in cell cycle entry and progression. To address this question, we calculated mutual information between individual and pairwise combinations of features of the FIRE reporter time series and cell cycle states. However, even

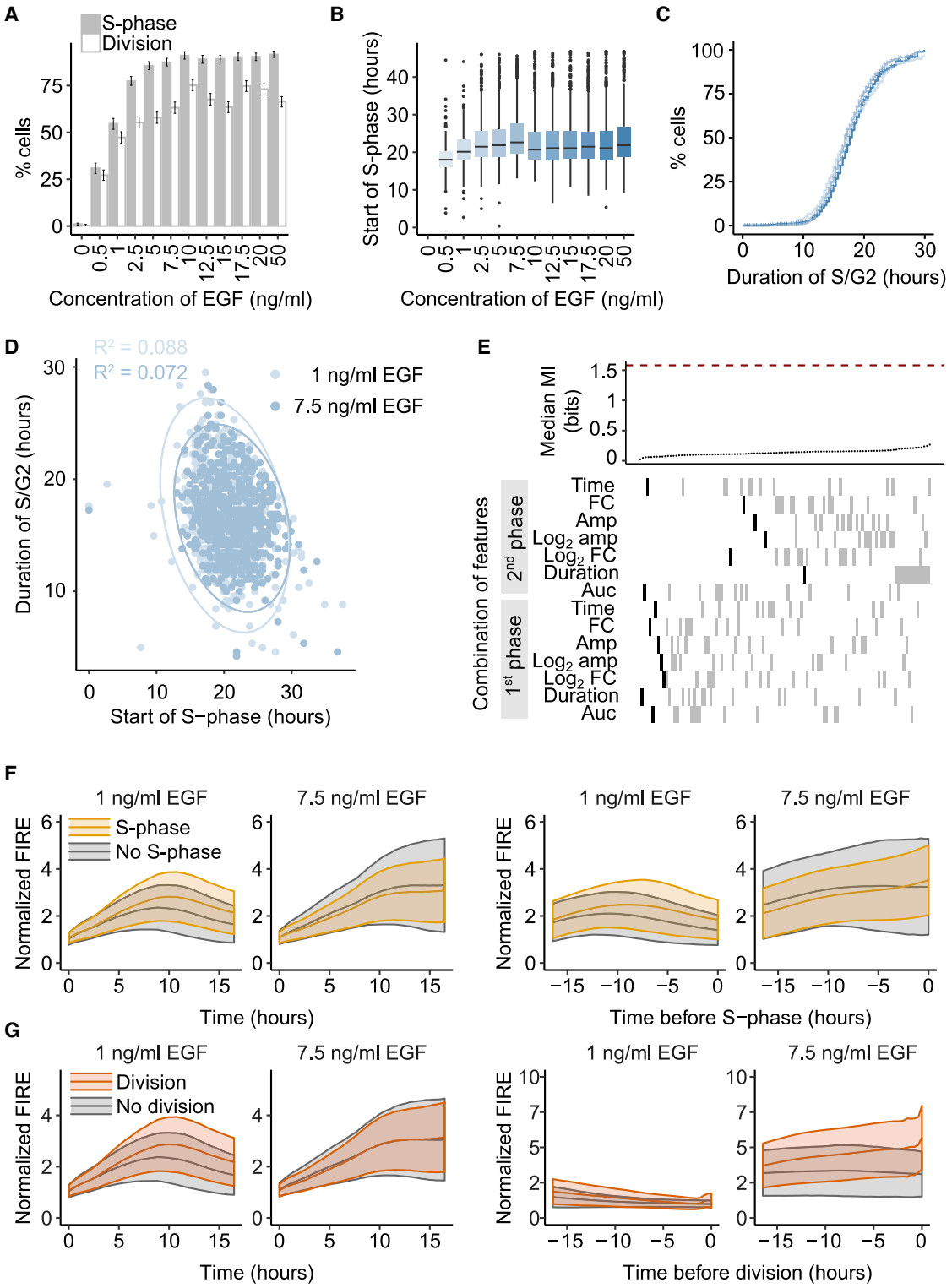

Figure 3. The Role of ERK Activity for Cell Cycle Entry and Progression

(A) Percentage of cells entering S phase (light gray) and dividing (dark gray) at indicated concentrations of EGF. Error bars indicate 95% confidence interval estimated with bootstrapping (n = 1,000).

(B) Distribution of the time at which S phase starts after stimulation with indicated concentrations of EGF.

(legend continued on next page)

the most informative feature combination provided only below 0.2 bits of mutual information (Figures 3E and S4J). Accordingly, when analyzing cells that have been treated with 1 ng/ml EGF, a concentration at which about 50% of the cells enter cell cycle, the median FIRE signal during the first response was only slightly higher in cells entering S phase than those that remained in G0/G1 phase, emphasizing that the FIRE signal has a very low predictive power for the cell cycle fate of a cell (Figure 3F). Similarly, actively replicating cells marked by EdU incorporation had only slightly higher FIRE levels at various time points (Figure S4I). At higher EGF concentrations, we also observed no noticeable differences in the shape and amplitude between cells entering S phase and those that did not (Figure 3F). Even when we align the single-cell FIRE trajectories to the time of S-phase entry to correct for asynchronies in the response and compared these trajectories to FIRE trajectories of quiescent cells aligned to a matched time distribution, we again detected only marginal differences (Figure 3F).

As we could not observe a strong correlation between FIRE levels and S-phase entry, we next analyzed if cell division was influenced by integrated ERK activity. Comparing the fold change in FIRE levels during the first response in dividing and non-dividing cells, we observed a similar trend as for S-phase entry (Figure 3G). Only when analyzing FIRE levels in the 16 h preceding cell division did we observe a more noticeable difference between cycling and quiescent cells. However, as this difference was only visible when cells were stimulated with high doses of EGF, the measurements did not provide support for a decisive influence of ERK signaling in the completion of the cell cycle. Most strikingly, integrated ERK activity was not elevated at low doses of EGF in the hours before division, suggesting that ERK activity might occur at late S phase when ligands are present but may not be required to complete the cell cycle. Taken together, our data corroborate that ERK activity is necessary for quiescent cells to re-enter the cell cycle, as previously reported (Sharrocks, 2006; Zhang and Liu, 2002), but they are insufficient to explain the variability of cellular responses, arguing for additional mitogenic inputs that are transmitted upon EGF stimulation.

PI3K Signaling Contributes a Necessary Mitogenic Stimulus upon EGF Treatment

To determine the extent to which the ERK/MAPK pathway transmits pro-mitotic signal from EGFR signaling, we systematically perturbed EGFR and components of the MAPK signaling pathway while monitoring integrated ERK activity, time of S-phase entry, and duration of the S/G2 phase (Figure 4A). Blocking the activity of EGFR by using the small-molecule inhibitor gefitinib abrogated all ERK signaling activity as well as cell cycle entry and progression (Figures 4B and 4D), reemphasizing that, in this model, EGFR signaling is absolutely essential for cell cycle entry. Time-series measurements of phosphoproteins showed that EGF stimulation activates ERK, AKT, and JNK signaling (Figure 4C; Table S1). Inhibiting the MAPK cascade with the MEK inhibitor AZD6244 led to a strong reduction of phospho-ERK and induction of MEK phosphorylation (Figure 4C), consistent with feedback regulation (Fritsche-Guenther et al., 2011; Klinger et al., 2013; Sturm et al., 2010). Although MEK inhibition prevented FIRE activation to a similar extent as the EGFR inhibitor (Figure 4B), about 10% of cells started cycling in this condition (Figure 4D). Interestingly, the duration of the S/G2 phase of those cells that entered the cell cycle was unaffected by the MEK inhibitor (Figure 4E).

Although pharmacological perturbation of the MAPK pathway highlighted its importance for cell cycle progression, MEK inhibition did not lead to a complete block of S-phase entry, in contrast to EGFR inhibition. This suggested that parallel pathways contribute significantly to mitogenic signaling. Therefore, we pharmacologically perturbed the interacting kinases p38 (SB203580), JNK (JNK inhibitor VI), and GSK3 (SB216763) as well (Figures 4B–4E; Table S2). JNK and GSK3 inhibition had no effect on ERK activity and led to only minor changes in the cellular response (Figures 4B–4E). However, we observed a marked increase in FIRE signals and MEK phosphorylation upon p38 inhibition as well as a reduction in AKT phosphorylation (Figures 4B and 4E). Interestingly, this did not lead to an increase in the fraction of cells entering S phase or dividing (Figure 4D). In contrast, we observed a longer duration of the S/G2 phase as well as a concomitant decrease in the number of cells dividing (Figures 4D–4E). This, again, indicates that ERK activity is not limiting for cell cycle regulation.

Finally, we inhibited the PI3K pathway by using pharmacological inhibitors. As the PI3K pathway is activated in parallel to MAPK signaling through the EGF receptor, it is an obvious candidate for transmitting additional mitogenic input. Indeed, inhibiting PI3K itself by using the inhibitor LY29402 led to a near-complete block of cell cycle entry and progression, and those few cells that entered the cell cycle had prolonged S/G2 phases (Figures 4D and 4E). As with p38 inhibition, ERK was still as active as in control cells, when assayed with the FIRE reporter (Figure 4B), although phosphorylation was broadly reduced across pathways. The effect of inhibiting the downstream kinase AKT with the small molecule MK-2206 was more restricted to this

(C) Estimates of the length of S/G2 phase distribution (time from beginning of S phase to division) for three different concentration of EGF (1, 7.5, and 50 ng/ml) using Kaplan-Meier analysis.
(D) Scatterplot comparing the time at which S phase starts after stimulation and length of S/G2 phase for two different concentrations of EGF (1 and 7.5 ng/ml). Ellipses indicate area that include 95% of the cells.
(E) Multivariate mutual information (top panel) between combinations of features of the FIRE reporter time series (as in Figure 2B) and cell cycle state. The red line indicates the theoretical maximum.
(F and G) Average (bold line) and standard deviation (ribbon) of reporter time series (normalized to unstimulated control) of cells entering S phase (yellow) and cells that do not enter S phase (gray) stimulated with indicated concentrations of EGF. Left graphs show the first 16.5 h after stimulation; right graphs show 16.5 h before the onset of S phase or equivalently sampled time series for non-responding cells (F). Comparison of dividing cells (orange) and non-dividing cells (gray) for the first 16.5 h after stimulation or before division (G).
See also Figure S4.

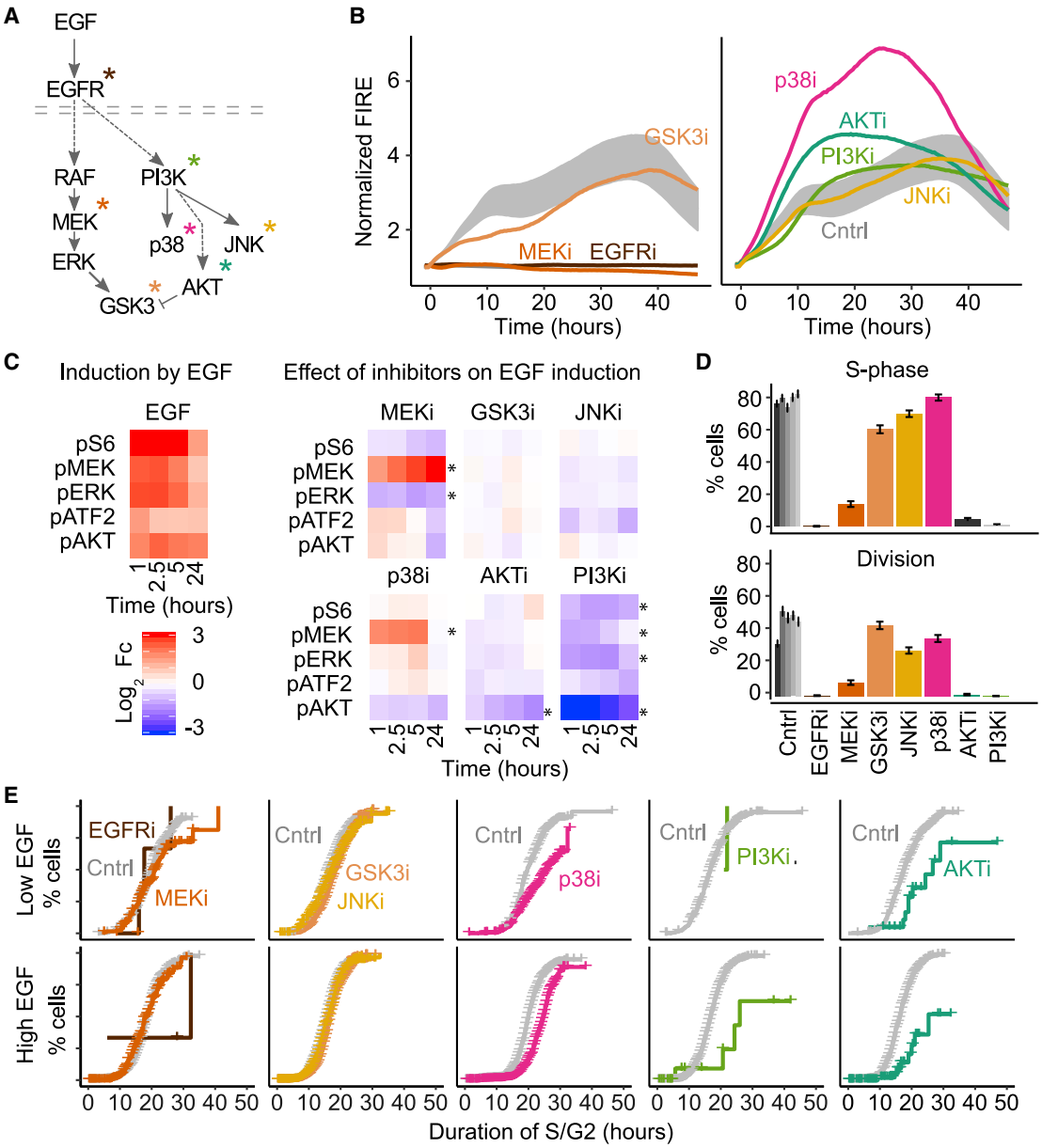

Figure 4. Pharmacological Perturbation Reveals Relative Contributions of ERK and PI3K/AKT Pathways during Mitogenic Signaling

(A) Scheme of the EGF pathway indicating the targets (colored asterisk) of pharmacological inhibitors used in this study. Dashed lines indicate indirect activation.

(B) Average time courses of the FIRE reporter after stimulation with EGF for controls (gray) and after pre-incubation with the indicated inhibitors. For controls, the standard deviation around the mean of five experiments is shown (gray ribbon).

(C) Effect of inhibitors on the phosphorylation state of targets in the MAPK and PI3K pathways. Changes in phosphorylation upon EGF stimulation (7.5 ng/ml) are shown for indicated time points compared to unstimulated control (left, mean $\log_2$ FC, n = 2). The effect of inhibitors is shown compared to the respective unperturbed time point after EGF stimulation (right). pS6, AKT substrate; pATF2, p38/JNK substrate. Significance of differences was tested using limma and significant differences ($p < 0.05$) were indicated with an asterisk.

(D) Effect of inhibitors on the percentage of cells entering S phase (top panel) or dividing (bottom panel) at the indicated concentration of EGF. Error bars indicate 95% confidence interval based on bootstrapping (n = 1,000).

(E) Effect of inhibitors on the duration of S/G2 phases for two different EGF (1 and 7.5 ng/ml) concentrations by using Kaplan-Meier analysis.

See also Figures S5A and S5D.

signaling branch when assayed on the level of phosphorylation and led to similar effects on the cell cycle as PI3K inhibition (Figures 4B–4F).

Interestingly, we observed increased FIRE levels upon PI3K and AKT inhibition. As blockage of PI3K, AKT, and p38 led to reduced cell cycle entry and increased FIRE activity, it was

conceivable that inhibited cell cycle progression might feed back into ERK signaling or might affect FIRE activity by different means. To test this hypothesis, we inhibited cell cycle progression by using the CDK4/6 inhibitor palbociclib and the CDK1 inhibitor RO3306. Although these inhibitors prevented S-phase entry and cell division, respectively, FIRE levels were not amplified, arguing against a direct influence of the cell cycle on ERK activity (Figures S5A–S5D).

Cell Cycle Entry and Progression Have Diverging Temporal Requirements for MAPK and PI3K Signaling

To gain a better understanding of the relative contribution of MAPK and PI3K signaling for regulating cell cycle entry and progression, we inhibited the corresponding pathways as well as EGFR activity at different time points during the first 20 h after growth factor stimulation (Figure 5A). When EGFR-dependent signaling was blocked entirely 10 h after EGF treatment by using the receptor inhibitor gefitinib, FIRE signals rapidly decayed and cell cycle entry was prevented in almost all cells (Figures 5B–5E). Sustaining EGFR activity for 15 or 20 h led to an increasing fraction of cells entering and progressing through the cell cycle. As expected, the duration of ERK activity was extended as well. We observed a similar abrogation of the FIRE response when we blocked the MAPK pathway at the level of MEK at different time points after EGF stimulation (Figure 5B; Gillies et al., 2017). However, more cells entered S phase when the MEK inhibitor was added at 10 h than gefitinib. Even more striking was the relative increase in cells dividing compared with EGFR inhibition at all time points tested (Figure 5C). In contrast, blocking PI3K signaling at 10, 15, or 20 h post-EGF treatment led to a comparable or even stronger suppression of S-phase entry and cell division as EGFR inhibition despite only temporarily attenuating ERK activity (Figures 5B and 5C). Inhibiting EGFR, MEK, or PI3K for different periods at the beginning of the experiment led to delayed FIRE accumulation and S-phase entry, as expected (Figures S5E, S5H, S5G, and S5J). However, cells still entered S phase in comparable numbers after inhibitors were washed away (Figures S5F and S5I). Only when inhibitors were applied for 15 h did the number of dividing cells decrease due to the limited observation period. These experiments corroborate that both ERK and PI3K activity are necessary for S-phase entry (Jones and Kazlauskas, 2001).

When we examined cells that progressed into S phase upon PI3K inhibition more closely, we noticed higher geminin levels at the time of treatment, indicating that they already passed the restriction point and initiated the transition from G1 to S phase prior to the loss of PI3K activity (Figure 5D). Importantly, we observed strongly increased durations of the S/G2 phase in cycling cell when we blocked PI3K signaling 10–20 h after EGF treatment (Figure 5E). The same decreased rate of cell cycle progression was observed upon EGFR inhibition, whereas preventing ERK activation had no effect once cells entered the cell cycle (Figure 5E).

To further study the important role of PI3K signaling for S- and G2-phase progression, we aimed to initiate ERK activity for a short period and then additionally activate PI3K by additional ligands. To do so, we used EGF at very low doses (0.1–0.5 ng/ml) that, due to ligand degradation, are expected to signal only transiently. We additionally stimulated cells with insulin-like growth factor (IGF), which preferentially activates AKT (Figure 6A). When assessing signaling activity by measuring phosphoproteins after stimulation with a high or low dose of EGF and a combination of low dose EGF and IGF, we confirmed that a low dose of EGF led to transient activation of many phosphoproteins, which peaked at 5 h (Figure 6B; Table S3). The addition of IGF induced increased phosphorylation of AKT and further downstream targets of PI3K, such as S6 or mTOR, throughout the first 24 h, while leaving other modifications unaltered. Using the FIRE reporter, we confirmed transient ERK activation at low doses of EGF that was unaffected by the addition of IGF (Figures 6C and S6C). Moreover, IGF treatment alone did not induce FIRE accumulation (Figure S6A). Although the transient input by EGF was sufficient to induce cell cycle entry in about 25% of cells (Figures 6D and S6D), these cells needed longer to complete S/G2 phase than cells with high EGF inputs (Figures 6E and S6E). However, when we combined low EGF input with IGF stimulation, which predominantly activates the PI3K pathway, it rescued the phenotype and resulted in cell cycle progression rates comparable to high EGF stimuli (Figures 6E and S6E). Importantly, IGF treatment alone did not result in appreciable cell cycle entry (Figure S6B), whereas a combination of low EGF and strong IGF inputs led to a modest increase in the fraction of cells entering S phase and dividing (Figures 6D and S6D). Consistently, actively replicating cells incorporating EdU showed a trend toward higher levels of phosphorylated AKT than those cells remaining in G1 upon treatment with both EGF alone and EGF together with IGF (Figures S6F and S6G). We obtained similar results when combining EGF at a low dose with insulin (Figures S6H–S6J).

To investigate the role of PI3K signaling during S and G2 phase, we stimulated cells with EGF and inhibited MEK and PI3K activity 15 h later. We then used single-cell RNA sequencing (scRNA-seq) to determine expression profiles of individual cells 20 h and 30 h after the addition of the growth factor (Figure 7A; STAR Methods). Visualization of the resulting data by dimensionality reduction using uniform manifold approximation and projection (UMAP) showed clear separation of quiescent and EGF-stimulated cells (Figure 7B, gray and blue dots). Inhibiting PI3K and, to a lesser extent, MEK led to distinct expression profiles that clustered separately from cells treated with EGF only (Figure 7B, green and red dots). Interestingly, expression profiles of inhibitor-treated cells differed at the 20-h and 30 h-time points. Similar results were obtained in a replicate experiment and by using a different dimensionality reduction method (principal-component analysis, Figures S7A and S7B). To correlate expression profiles of individual cells with cell cycle progression, we mapped the cell cycle state of each cell by using characterized marker genes (Stuart et al., 2019; STAR Methods). This allowed us to determine cell cycle distributions for each condition and time point that were comparable to previous analysis using time-lapse microscopy (Figure S7C). Combining the UMAP projection with cell cycle information revealed a clear progression of EGF-stimulated cells from G1 to S and G2/M phase (compare Figures 7B and C). Importantly, cells progressing into S and G2/M phase in the presence of PI3K and MEK inhibitors showed clearly distinguishable expression profiles. Using the pathway activity scores calculated by the PROGENy method

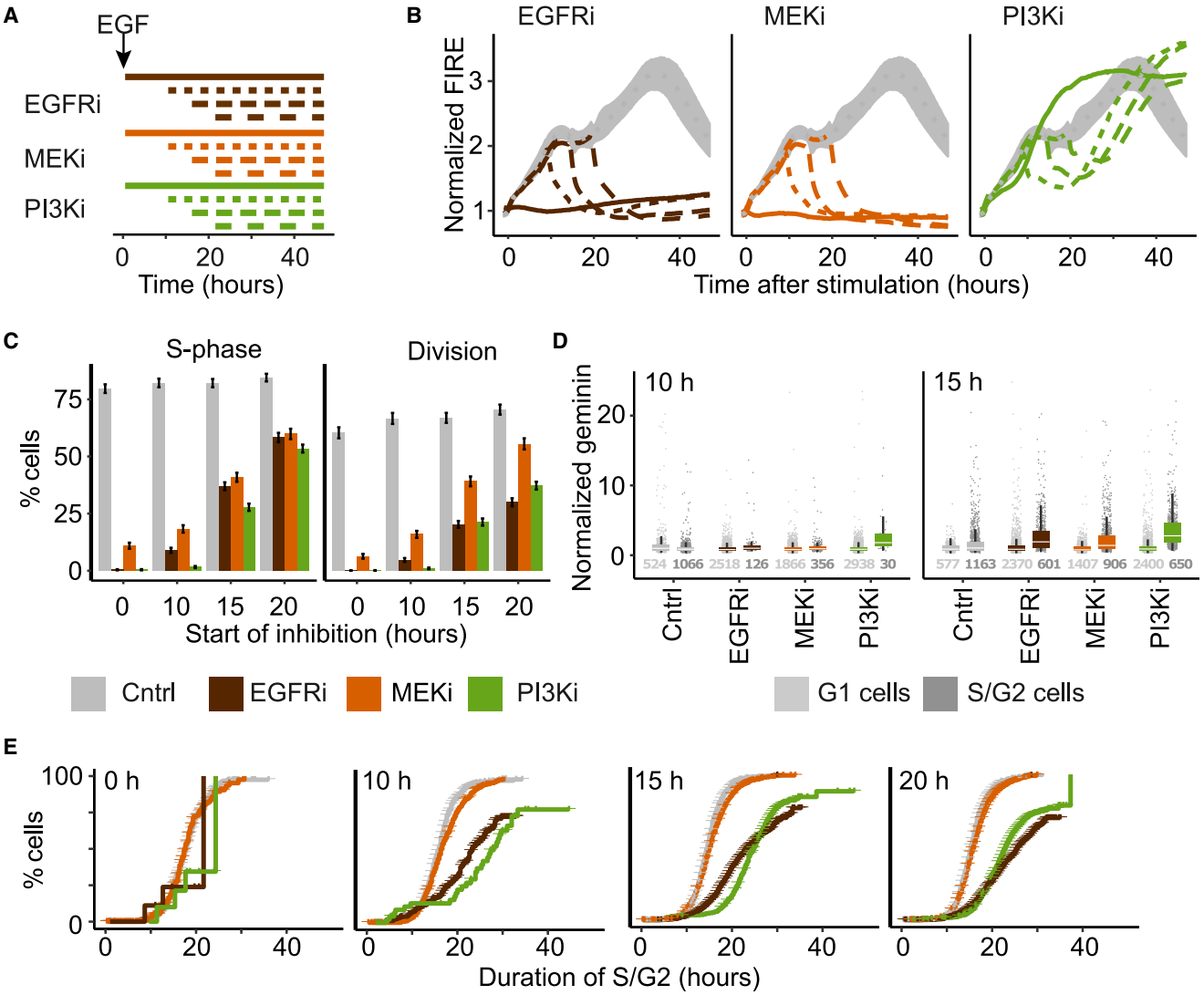

Figure 5. Temporal Requirements for ERK and AKT Activity Differ during Cell Cycle Progression

(A) Scheme of experiment. EGFR, MEK, and PI3K inhibitors were added either at time of stimulation or 10, 15, or 20 h after stimulation.

(B) Average time courses of the FIRE reporter after stimulation with 7.5 ng/ml EGF and incubation with the indicated pharmacological inhibitors at different time points or controls (gray). For controls, the standard deviation around the mean of three experiments is shown (gray ribbon).

(C) Effect of inhibitors on the percentage of cells entering S phase (left) or dividing (right) for the indicated time of inhibition after stimulation. Error bars indicate 95% confidence interval based on bootstrapping (n = 1,000).

(D) Comparison of geminin levels at time of inhibitor treatment (as indicated) between cells entering S phase (right, dark gray) and cells that do not enter S phase (left, light gray) within the time of measurement. Numbers of cells for each condition are indicated.

(E) Effect of the time of inhibitor treatment (as indicated) on the duration of S/G2 phases after stimulation with 7.5 ng/ml EGF compared to controls using Kaplan-Meier analysis.

See also Figures S5E–S5J.

(Schubert et al., 2018), we validated that inhibitor treatment led to the expected changes in MAPK and PI3K signaling (Figure S7D). Next, we determined differentially expressed genes upon inhibitor treatment depending on cell cycle state and time point and resolved the corresponding molecular pathways using Gene Ontology (GO) term analysis (Figure S7E). In G1-phase cells, we mainly observed changes in the expected molecular pathways, such as response to growth factors. In S-phase cells, only PI3K-inhibitor -treated cells showed significant changes, which mainly affected pathways involved in metabolic processes, such as mitochondrial respiration, translation, and ribonucleotide synthesis. In G2/M-phase cells at 30-h post-EGF stimulation, MEK and PI3K inhibition induced distinct alterations in pathway activity. For PI3K inhibition, changes in G2/M-phase cells partially overlapped with those observed during S phase.

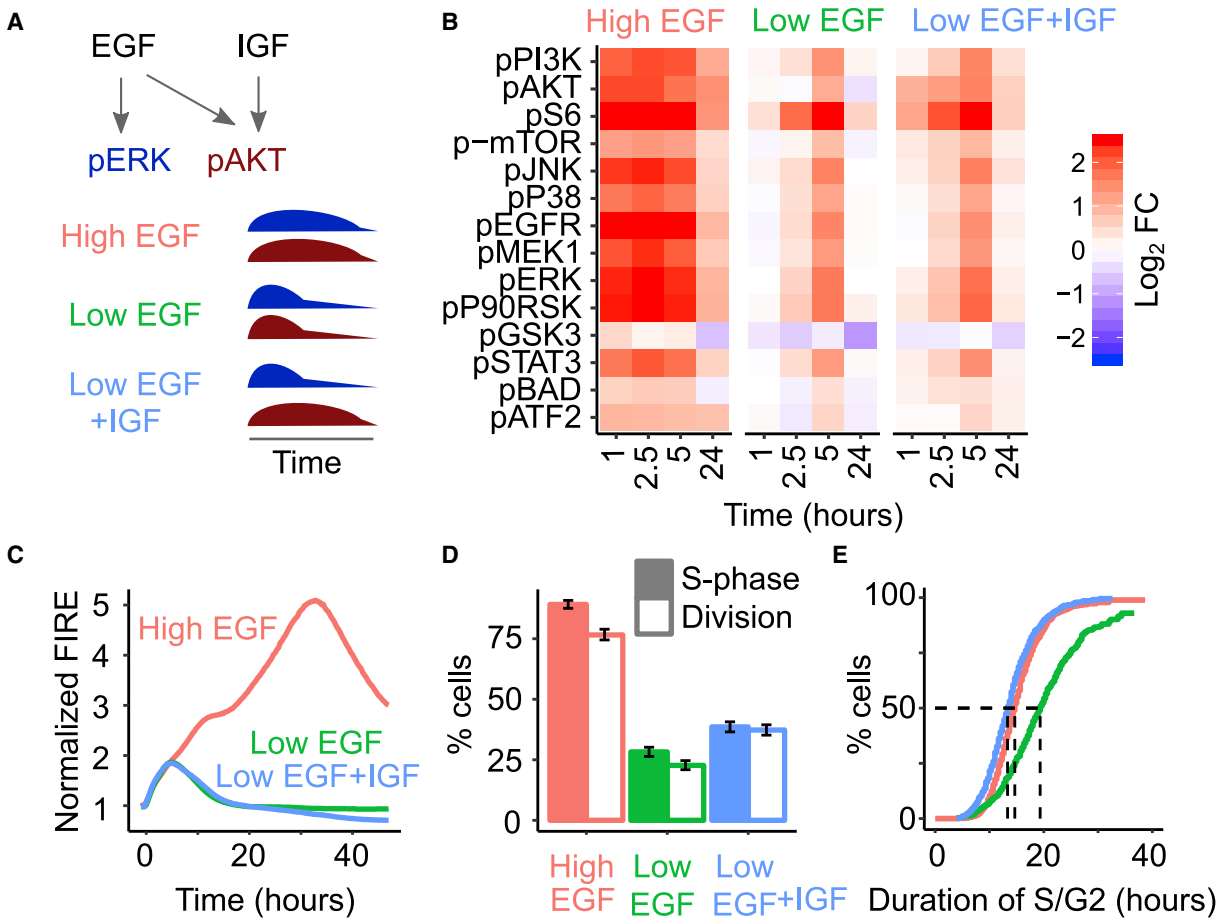

Figure 6. AKT Activation Rescued Delayed Cell Cycle Progression at Low EGF Concentrations

(A) Pathway scheme of the EGF and IGF pathways and overview of the performed rescue experiment.

(B) Effect of low and high doses of EGF stimulation (0.5 ng/ml and 50 ng/ml) as well as IGF co-stimulation on the phosphorylation state of targets in the MAPK and PI3K pathway. Changes in phosphorylation are shown for four time points compared to unstimulated control (mean $\log_2$ FC, n = 2). p-mTOR, BAD-AKT substrates; pSTAT3, pP90RSK-ERK substrates

(C) Average time courses of the FIRE reporter after stimulation with different concentrations of EGF as well as co-stimulation with IGF.

(D) Percentage of cells entering S phase (solid bars) or dividing (open bars) after stimulation. Error bars indicate 95% confidence interval based on bootstrapping (n = 1,000).

(E) Duration of S/G2 phase using Kaplan-Meier analysis.

See also Figure S6.

To determine whether the observed delay in cell cycle progression upon PI3K inhibition was due to an increased duration of S or G2/M phase, we further analyzed cell cycle distributions from scRNA-seq. As expected, we observed a decreased fraction of cells in S, G2, or M phase 20 h after EGF treatment when MEK or PI3K activity was inhibited 15-h post-stimulation (Figure 7D, top graph). The fraction of S/G2M-phase cells further decreased at the 30-h time point, as no additional cells could enter S phase in the absence of MAPK or PI3K activity, whereas others successfully progressed through the cell cycle and divided. When we analyzed the ratio between S- and G2/M-phase cells under both conditions, we observed that most MEK-inhibitor-treated cells completed S phase between the 20-h and 30-h time point (Figure 7D, bottom graph). However, upon PI3K inhibition, a noticeable fraction of cells remained in S phase at the 30-h time point, indicating a delay in S-phase progression.

To support this conclusion, we monitored FIRE reporter cells upon EGF treatment by time-lapse microscopy, inhibited MEK and PI3K activity after 15 h, and performed metabolic labeling with EdU at 22.5-h and 32.5-h post-stimulation, respectively (Figure 7E). Consistent with our scRNA-seq analysis, we observed that most geminin-positive cells were actively replicating at the 22.5-h time point (Figure 7F). After 32.5 h, MEK-inhibitor-treated cells completed S phase and entered G2 phase. Under control conditions, we still observed some replicating cells at this time point, as cells were still able to enter S phase from G1. However, although no additional cells were able to enter S phase upon PI3K inhibition, we observed that most treated cells still incorporated EdU at the later time point. To estimate the corresponding

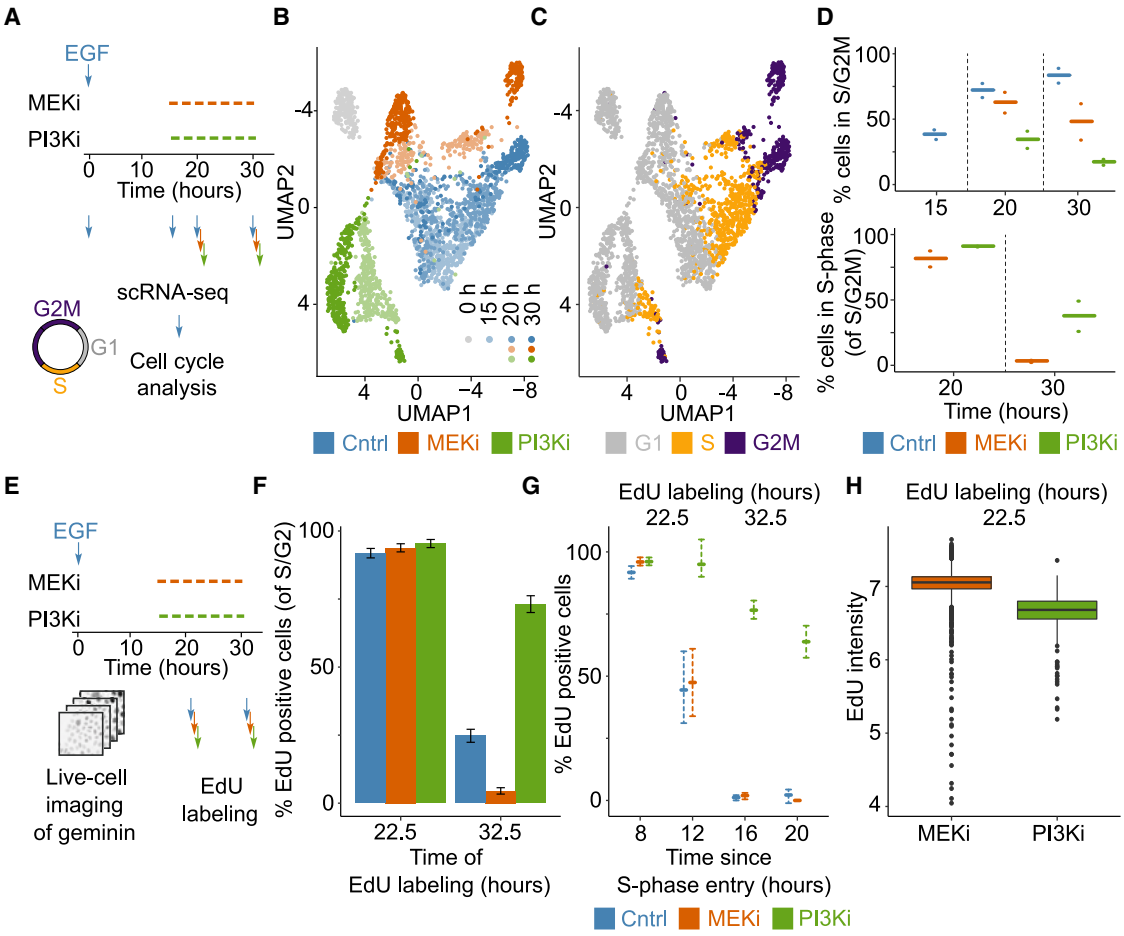

Figure 7. PI3K Signaling Is Required for Timely Progression through S Phase

(A) Scheme of single-cell RNA sequencing experiments. Cells were stimulated with 7.5 ng/ml EGF. MEK or PI3K inhibitors were added after 15 h and cells were sampled for single-cell RNA sequencing at the indicated time points.

(B) UMAP for one experiment. Cells are barcoded for experimental condition.

(C) UMAP as in (B) with cells barcoded for cell cycle phases.

(D) Percentage of cells in S/G2M phase (top panel) based on cell cycle markers (dots, replicates; lines, mean). Effect of MEK or PI3K inhibitors, respectively, on percentage of cells in S phase (bottom panel).

(E) Scheme of live-cell imaging experiments with EdU stainings at different time points.

(F) Percent of EdU-positive cells that started S phase before EdU staining based on analysis of geminin levels. Error bars indicate 95% confidence interval based on bootstrapping (n = 1,000).

(G) Effect of MEK or PI3K inhibitor on the number of EdU-positive cells labeled at indicated time points. Cells were binned according to the time since entering S phase (based on geminin). Error bars indicate 95% confidence interval based on bootstrapping (n = 1,000).

(H) Effect of MEK (orange) and PI3K inhibitor (green) on the extent of EdU incorporation.

See also Figure S7.

time of S-phase progression, we binned cells according to the time of S-phase entry, as indicated by geminin accumulation relative to the time of metabolic labeling, and determined the corresponding fraction of EdU-positive cells (Figure 7G). Although control and MEK-inhibitor-treated cells completed S phase within 16 h, most cells remained in S phase for over 20 h in the absence of PI3K activity. This severe delay in S-phase progression was further supported by a slower rate of EdU label incorporation in PI3Ki- than in MEK-inhibitor-treated cells (Figure 7H).

Taken together, quantitative time-resolved analysis at the single-cell level showed that the mitogenic input of EGF ligands is transmitted both by the MAPK and PI3K signaling pathway. Activation of both pathways together is necessary for cell cycle entry. However, timely progression through S phase depends on sustained PI3K signaling to adjust the metabolism of the cell to the replicative state.

DISCUSSION

Mitogenic signaling allows multicellular organisms to regulate the rate and timing of cell division. To ensure precise control over cell cycle entry and progression, the information flow

through multiple signaling pathways needs to be integrated dynamically to coordinate the different components of the cell cycle machinery (Chambard et al., 2007). Combining time-resolved measurements in individual cells with computer-aided data analysis, information theoretical calculations and pharmacological perturbations allowed us to disentangle the contributions of the MAPK and PI3K/AKT pathways to mitogenic signaling during different phases of the cell cycle.

To measure signaling activity, we used live-cell microscopy of fluorescent reporter cells. In addition to unrivaled temporal resolution, live-cell microscopy allows resolving non-genetic heterogeneity that can strongly influence the outcome of signaling events (Spiller et al., 2010). Several strategies have been developed to monitor MAPK pathway activity in living cells: FRET-based reporters allow direct measurements of substrate phosphorylation but are limited by a low signal-to-noise ratio and are prone to saturation (Gillies et al., 2017; Komatsu et al., 2011; Ryu et al., 2015; Selimkhanov et al., 2014). Translocation-based reporters provide a similar but more robust ratiometric measure (Regot et al., 2014). However, their sensitivity is also restricted to certain segments of the ERK dynamic range (Gillies et al., 2017). Nuclear localization of an ERK-yellow fluorescent protein (YFP) fusion correlates with its activity on short timescales but can be affected by other cellular processes (Cohen-Saidon et al., 2009). Finally, as we were interested in understanding how and when total ERK activity affected cell cycle progression, we decided to use the FIRE reporter that linearly reflects integrated ERK activity (Albeck et al., 2013; Gillies et al., 2017). Although the FIRE reporter does not allow us to directly follow the short-term dynamics of ERK activity observed with other reporters, it provides a robust readout that enabled us to faithfully measure the contribution of MAPK signaling over the long timescales involved in progressing from a quiescent state to cell division. When comparing our measurements to previously reported data from Albeck et al. (2013), it is important to keep in mind that different experimental conditions were used. Although previous studies focused on steady-state EGF signaling under sustained stimulations, we investigated the response of quiescent cells to acute growth factor stimulation. Also, as the FIRE reporter captures only nuclear activity, we could not consider signaling effects of the MAPK pathway that take place in the cytoplasm (Murphy et al., 2002). This might explain why under some conditions, such as PI3K and AKT inhibition, FIRE response and phosphorylation diverge. Furthermore, the use of a synthetic reporter such as FIRE may introduce additional variability that could potentially degrade measurements of information flow and mask correlations in individual cells. As an alternative, measurements of endogenously tagged ERK targets, such as FRA1, may be used (Gillies et al., 2017).

Using automated image analysis, we extracted a time series of ERK activity over 2 days for thousands of cells treated with various concentrations of EGF. Information theoretical calculations allowed us to identify the features of the dynamic ERK response that conveyed the most information about extracellular EGF concentrations. In recent years, information theory has been increasingly used to investigate principles of signal transduction or to quantitatively compare signaling pathways (Brennan et al., 2012; Mc Mahon et al., 2014). Analysis of tumor necrosis factor alpha (TNFα)-induced nuclear factor κB (NF-κB) signaling at a single time point, for example, indicated that information transmission through the network is restricted by molecular noise and, therefore, limits the ability of a cell to derive precise information about ligand concentrations (mutual information, <1 bit) (Cheong et al., 2011). Similar low capacities to transmit information were observed for other pathways, including calcium, cyclic AMP (cAMP), and MAPK signaling (Garner et al., 2016; Selimkhanov et al., 2014; Uda et al., 2013; Voliotis et al., 2014). However, estimating information flow from a limited number of measurements at arbitrarily selected points of the underlying molecular networks has its limitations. For example, restrictions on information transmission can be mitigated by integrating temporal information or modulating feedback strength (Garner et al., 2016; Voliotis et al., 2014).

Our analysis confirms that when considering appropriate dynamic features, mutual information above 1 bit can be obtained. We used information theory to systematically probe which features of the reporter time series carry the most information. This analysis showed that the combination of fold changes of the first and second response of the biphasic ERK activity profile convey the most information about extracellular ligand concentration. Our continuous measurements from unperturbed individual cells, thus, confirmed previous observations from biochemical studies of cell populations (Meloche et al., 1992). From these data, it was proposed that initial ERK activity is necessary to mediate the transition from the G0 state of the cell cycle to G1. During G1 phase, reduced nuclear ERK activity promotes cell cycle progression, as the transcription factor FOS is degraded and replaced by FRA1 (Burch et al., 2004). Sufficiently strong activation of ERK during late G1 phase is finally necessary to induce transcription factors, such as EGR1, which mediate the all-or-none decision to enter S phase and divide (Zwang et al., 2011). Using pharmacological inhibitors to artificially abbreviate ERK activity, we could confirm that some level of ERK signaling is required for S-phase entry (Figure 5). However, we did not detect a clear correlation between ERK activity and S-phase entry at low EGF doses in simultaneous measurements of FIRE and cell cycle reporters (Figure 3F). Consistently, there was no direct correlation between S-phase entry and the occurrence of a second signaling phase (Figures 1E and 3A). We, therefore, hypothesize that entering S phase is similar to a stochastic decision that requires sustained ERK activity. Depending on the duration of G1 phase, transient ERK signaling may suffice in one cell, whereas both phases of ERK signaling may be required in another one. A corresponding threshold mechanism could be based on EGR1 induction and convert the graded input of ERK activation into a digital decision to pass the restriction point (Zwang et al., 2011) .

The observed heterogeneity in S-phase entry may be due to varying levels of cell cycle inhibitors, such as p21. In elegant single-cell experiments, it was shown that the decision between proliferation and quiescence in cycling MCF10A cells is controlled by a bifurcation in CDK2 activity due to varying levels of p21 as a consequence of endogenous DNA damage during replication (Arora et al., 2017; Barr et al., 2017; Spencer et al., 2013). It will now be interesting to investigate if heterogeneity

in p21 persists during growth-factor-starvation-induced quiescence or if other molecular mechanisms are involved in the observed heterogeneous responses to low EGF concentrations. For example, it is conceivable that heterogeneous expression of inhibitors of the PI3K pathway, which we showed to be required for cell cycle entry as well, contributes to the proliferation-quiescence decision.

In addition to quantifying the decision to enter cell cycle, we followed the phenotypic response of each cell to determine the frequency and timing of cell division. By integrating molecular measurements of post-translational modifications as well as pharmacological perturbations, we showed that ERK signaling is dispensable after crossing of the restriction point, whereas PI3K/AKT activity was necessary both for entering S phase and for timely progression to mitosis. However, activation of AKT through IGF or insulin alone was insufficient to induce cell cycle entry. During G1, it is known that ERK and AKT signaling interact at the level of cell cycle inhibitors, although the precise effects may depend on the cell line studied (Worster et al., 2012; Zwang et al., 2011). Our data from pharmacological inhibition at different intervals after stimulation show that after PI3K inhibition, no further cells enter S phase, whereas with MEK inhibition, some cells still enter S phase. This is consistent with previous studies, which showed that progression through G1 requires PI3K/AKT and ERK signaling, whereas S-phase entry itself is mainly dependent on PI3K/AKT (Jones and Kazlauskas, 2001). As AKT activity can suppress anti-proliferative gene products induced during early G1 phase, it may render cells permissive for ERK-driven S-phase entry (Zwang et al., 2011). AKT's role in controlling progression through S/G2 phase is less well documented. It was shown that blocking PI3K/AKT signaling prolongs progression through S/G2, although it remained unclear if S phase or G2 phase is prolonged (Dangi et al., 2003). Our data from scRNA-seq and life-cell imaging combined with metabolic labeling show that inhibition of AKT signaling strongly prolongs S phase. One proposed mechanism is that AKT phosphorylates CDK2 and regulates its subcellular localization during S phase (Maddika et al., 2008). The resulting AKT-induced nucleo-cytoplasmic shuttling of CDK2 may be necessary for cell cycle progression. In further studies, it may be interesting to measure AKT activity and CDK2 localization simultaneously in living cells. Additionally, metabolic demands of S phase may require high AKT signaling. The AKT signaling pathway is a key regulator of cellular metabolism, including glycolysis and nucleotide biosynthesis (Ward and Thompson, 2012). Analysis of the differentially expressed genes in our scRNA-seq data showed that, indeed, PI3K blockage deregulates genes involved in metabolic processes during S phase. This provides evidence that unmet metabolic demand might contribute to prolonged S-phase progression in the absence of AKT signaling. In addition, AKT signaling also influences cell growth by mTOR signaling (Ward and Thompson, 2012), and cell size, in turn, might influence the length of S phase (Lloyd, 2013). However, it is currently unknown if and how cell size and cell cycle are coupled (Lloyd, 2013).

Perturbations of the signaling processes controlling cell cycle progression can be involved in severe pathologies. Amplification of EGF receptors in breast cancer cells, for example, increase mitogenic input to both ERK and PI3K/AKT signaling pathways. Alterations in the E2F/Rb system or loss of cell cycle inhibitors renders cells more permissive to ERK signaling. Mutations in the PI3K pathway, such as PTEN deletion, lead to increased AKT activity. Although single perturbations will not lead to changes in cell proliferation in most cases, the accumulation of alterations observed during tumorigenesis increase information flow through both mitogenic pathways and cause hypersensitivity to growth factors. Conversely, a detailed understanding of temporal requirements for and synergies between major mitogenic mechanisms may enable us to devise therapeutic interventions that counteract altered cell signaling. Rationally designed schedules of combination therapies may provide more efficiency in targeting both cycling and quiescent cells than continuous treatment with single agents, such as gefitinib. Further studies combining quantitative experimental data with computer-aided analysis will provide the necessary molecular insights for such next-generation therapies.

STAR★METHODS

Detailed methods are provided in the online version of this paper and include the following:

- KEY RESOURCES TABLE
- LEAD CONTACT AND MATERIALS AVAILABILITY
  - Lead Contact
  - Materials Availability
  - Data and Code Availability
- EXPERIMENTAL MODEL AND SUBJECT DETAILS
  - Cell lines
- METHOD DETAILS
  - Luminex assays
  - Live-cell microscopy experiments
  - EdU staining
  - Immunofluorescence
  - Single cell preparation for scRNA sequencing
  - Rehydration and library preparation
- QUANTIFICATION AND STATISTICAL ANALYSIS
  - Single cell RNA sequencing analysis
  - Data analysis of live-cell experiments
  - Clustering
  - Feature analysis
  - Information theoretical analysis
  - Kaplan-Meier analysis
  - Analysis of Luminex experiment with inhibitors
  - Analysis of EGF concentration

SUPPLEMENTAL INFORMATION

Supplemental Information can be found online at https://doi.org/10.1016/j.celrep.2020.03.078.

ACKNOWLEDGMENTS

We thank John Albeck (UC Davis) for sharing the FIRE reporter, Dhana Friedrich for performing initial experiments, Marcel Jentsch for help with image and data analysis, and members of the Blüthgen and Loewer labs for helpful discussion. We thank the BIMSB-MDC genomics core unit for support. This work was, in part, funded by the German Research Foundation (DFG) within the priority program SPP1395 InKoMBio (to N.B. and A.L.) and by the German

Ministry for Education and Research (BMBF), grants PREDICT (031L0023B, N.B.) and ZiSS-Trans (02NUK047E, N.B.).

AUTHOR CONTRIBUTIONS

S.B., M.L., and I.N. performed experiments; M.B. performed data analysis; M.B., N.B., and A.L. wrote the manuscript with contributions from all authors; and N.B. and A.L. conceived the study and supervised the research.

DECLARATION OF INTERESTS

The authors declare no competing interests.

Received: July 19, 2019
Revised: February 19, 2020
Accepted: March 23, 2020
Published: April 14, 2020

REFERENCES

Albeck, J.G., Mills, G.B., and Brugge, J.S. (2013). Frequency-modulated pulses of ERK activity transmit quantitative proliferation signals. Mol. Cell *49*, 249–261.

Arora, M., Moser, J., Phadke, H., Basha, A.A., and Spencer, S.L. (2017). Endogenous Replication Stress in Mother Cells Leads to Quiescence of Daughter Cells. Cell Rep. *19*, 1351–1364.

Barr, A.R., Cooper, S., Heldt, F.S., Butera, F., Stoy, H., Mansfeld, J., Novák, B., and Bakal, C. (2017). DNA damage during S-phase mediates the proliferation-quiescence decision in the subsequent G1 via p21 expression. Nat. Commun. *8*, 14728.

Bewick, V., Cheek, L., and Ball, J. (2004). Statistics review 12: survival analysis. Crit. Care *8*, 389–394.

Brennan, M.D., Cheong, R., and Levchenko, A. (2012). Systems biology. How information theory handles cell signaling and uncertainty. Science *338*, 334–335.

Burch, P.M., Yuan, Z., Loonen, A., and Heintz, N.H. (2004). An extracellular signal-regulated kinase 1- and 2-dependent program of chromatin trafficking of c-Fos and Fra-1 is required for cyclin D1 expression during cell cycle reentry. Mol. Cell. Biol. *24*, 4696–4709.

Carpenter, A.E., Jones, T.R., Lamprecht, M.R., Clarke, C., Kang, I.H., Friman, O., Guertin, D.A., Chang, J.H., Lindquist, R.A., Moffat, J., et al. (2006). CellProfiler: image analysis software for identifying and quantifying cell phenotypes. Genome Biol. *7*, R100–R111.

Chambard, J.-C., Lefloch, R., Pouysségur, J., and Lenormand, P. (2007). ERK implication in cell cycle regulation. Biochim. Biophys. Acta *1773*, 1299–1310.

Chen, J.-Y., Lin, J.-R., Cimprich, K.A., and Meyer, T. (2012). A two-dimensional ERK-AKT signaling code for an NGF-triggered cell-fate decision. Mol. Cell *45*, 196–209.

Cheong, R., Rhee, A., Wang, C.J., Nemenman, I., and Levchenko, A. (2011). Information transduction capacity of noisy biochemical signaling networks. Science *334*, 354–358.

Clijsters, L., Ogink, J., and Wolthuis, R. (2013). The spindle checkpoint, APC/C(Cdc20), and APC/C(Cdh1) play distinct roles in connecting mitosis to S phase. J. Cell Biol. *201*, 1013–1026.

Cohen, A.A., Geva-Zatorsky, N., Eden, E., Frenkel-Morgenstern, M., Issaeva, I., Sigal, A., Milo, R., Cohen-Saidon, C., Liron, Y., Kam, Z., et al. (2008). Dynamic proteomics of individual cancer cells in response to a drug. Science *322*, 1511–1516.

Cohen-Saidon, C., Cohen, A.A., Sigal, A., Liron, Y., and Alon, U. (2009). Dynamics and variability of ERK2 response to EGF in individual living cells. Mol. Cell *36*, 885–893.

Dangi, S., Cha, H., and Shapiro, P. (2003). Requirement for phosphatidylinositol-3 kinase activity during progression through S-phase and entry into mitosis. Cell. Signal. *15*, 667–675.

Dong, J., Peng, J., Zhang, H., Mondesire, W.H., Jian, W., Mills, G.B., Hung, M.-C., and Meric-Bernstam, F. (2005). Role of glycogen synthase kinase 3beta in rapamycin-mediated cell cycle regulation and chemosensitivity. Cancer Res. *65*, 1961–1972.

Fritsche-Guenther, R., Witzel, F., Sieber, A., Herr, R., Schmidt, N., Braun, S., Brummer, T., Sers, C., and Blüthgen, N. (2011). Strong negative feedback from Erk to Raf confers robustness to MAPK signalling. Mol. Syst. Biol. *7*, 489.

Garner, K.L., Perrett, R.M., Voliotis, M., Bowsher, C., Pope, G.R., Pham, T., Caunt, C.J., Tsaneva-Atanasova, K., and McArdle, C.A. (2016). Information Transfer in Gonadotropin-releasing Hormone (GnRH) Signaling: Extracellular signal-regulated kinase (ERK)-mediated feedback loops control hormone sensing. J. Biol. Chem. *291*, 2246–2259.

Gillies, T.E., Pargett, M., Minguet, M., Davies, A.E., and Albeck, J.G. (2017). Linear Integration of ERK Activity Predominates over Persistence Detection in Fra-1 Regulation. Cell Syst. *5*, 549–563.e5.

Harbour, J.W., and Dean, D.C. (2000). The Rb/E2F pathway: expanding roles and emerging paradigms. Genes Dev. *14*, 2393–2409.

Hay, N., and Sonenberg, N. (2004). Upstream and downstream of mTOR. Genes Dev. *18*, 1926–1945.

Heinrich, R., Neel, B.G., and Rapoport, T.A. (2002). Mathematical models of protein kinase signal transduction. Mol. Cell *9*, 957–970.

Jones, S.M., and Kazlauskas, A. (2001). Growth-factor-dependent mitogenesis requires two distinct phases of signalling. Nat. Cell Biol. *3*, 165–172.

Klinger, B., Sieber, A., Fritsche-Guenther, R., Witzel, F., Berry, L., Schumacher, D., Yan, Y., Durek, P., Merchant, M., Schäfer, R., et al. (2013). Network quantification of EGFR signaling unveils potential for targeted combination therapy. Mol. Syst. Biol. *9*, 673, 673.

Komatsu, N., Aoki, K., Yamada, M., Yukinaga, H., Fujita, Y., Kamioka, Y., and Matsuda, M. (2011). Development of an optimized backbone of FRET biosensors for kinases and GTPases. Mol. Biol. Cell *22*, 4647–4656.

Leung, J.Y., Ehmann, G.L., Giangrande, P.H., and Nevins, J.R. (2008). A role for Myc in facilitating transcription activation by E2F1. Oncogene *27*, 4172–4179.

Lloyd, A.C. (2013). The regulation of cell size. Cell *154*, 1194–1205.

Love, M.I., Huber, W., and Anders, S. (2014). Moderated estimation of fold change and dispersion for RNA-seq data with DESeq2. Genome Biol. *15*, 550.

Maddika, S., Ande, S.R., Wiechec, E., Hansen, L.L., Wesselborg, S., and Los, M. (2008). Akt-mediated phosphorylation of CDK2 regulates its dual role in cell cycle progression and apoptosis. J. Cell Sci. *121*, 979–988.

Marshall, C.J. (1995). Specificity of receptor tyrosine kinase signaling: transient versus sustained extracellular signal-regulated kinase activation. Cell *80*, 179–185.

Mc Mahon, S.S., Sim, A., Filippi, S., Johnson, R., Liepe, J., Smith, D., and Stumpf, M.P.H. (2014). Information theory and signal transduction systems: from molecular information processing to network inference. Semin. Cell Dev. Biol. *35*, 98–108.

Meloche, S., Seuwen, K., Pagès, G., and Pouysségur, J. (1992). Biphasic and synergistic activation of p44mapk (ERK1) by growth factors: correlation between late phase activation and mitogenicity. Mol. Endocrinol. *6*, 845–854.

Moelling, K., Schad, K., Bosse, M., Zimmermann, S., and Schweneker, M. (2002). Regulation of Raf-Akt Cross-talk. J. Biol. Chem. *277*, 31099–31106.

Murphy, L.O., Smith, S., Chen, R.-H., Fingar, D.C., and Blenis, J. (2002). Molecular interpretation of ERK signal duration by immediate early gene products. Nat. Cell Biol. *4*, 556–564.

Regot, S., Hughey, J.J., Bajar, B.T., Carrasco, S., and Covert, M.W. (2014). High-sensitivity measurements of multiple kinase activities in live single cells. Cell *157*, 1724–1734.

Rubinfeld, H., and Seger, R. (2005). The ERK cascade: a prototype of MAPK signaling. Mol. Biotechnol. *31*, 151–174.

Ryu, H., Chung, M., Dobrzyński, M., Fey, D., Blum, Y., Lee, S.S., Peter, M., Kholodenko, B.N., Jeon, N.L., and Pertz, O. (2015). Frequency modulation of ERK activation dynamics rewires cell fate. Mol. Syst. Biol. *11*, 838.

Sakaue-Sawano, A., Kurokawa, H., Morimura, T., Hanyu, A., Hama, H., Osawa, H., Kashiwagi, S., Fukami, K., Miyata, T., Miyoshi, H., et al. (2008). Visualizing spatiotemporal dynamics of multicellular cell-cycle progression. Cell *132*, 487–498.

Schmidt, M., Fernandez de Mattos, S., van der Horst, A., Klompmaker, R., Kops, G.J.P.L., Lam, E.W.-F., Burgering, B.M.T., and Medema, R.H. (2002). Cell cycle inhibition by FoxO forkhead transcription factors involves downregulation of cyclin D. Mol. Cell. Biol. *22*, 7842–7852.

Schubert, M., Klinger, B., Klünemann, M., Sieber, A., Uhlitz, F., Sauer, S., Garnett, M.J., Blüthgen, N., and Saez-Rodriguez, J. (2018). Perturbation-response genes reveal signaling footprints in cancer gene expression. Nat. Commun. *9*, 20.

Seger, R., and Krebs, E.G. (1995). The MAPK signaling cascade. FASEB J. *9*, 726–735.

Selimkhanov, J., Taylor, B., Yao, J., Pilko, A., Albeck, J., Hoffmann, A., Tsimring, L., and Wollman, R. (2014). Systems biology. Accurate information transmission through dynamic biochemical signaling networks. Science *346*, 1370–1373.

Shankaran, H., Ippolito, D.L., Chrisler, W.B., Resat, H., Bollinger, N., Opresko, L.K., and Wiley, H.S. (2009). Rapid and sustained nuclear-cytoplasmic ERK oscillations induced by epidermal growth factor. Mol. Syst. Biol. *5*, 332.

Sharrocks, A.D. (2006). Cell cycle: sustained ERK signalling represses the inhibitors. Curr. Biol. *16*, R540–R542.

Snijder, B., and Pelkmans, L. (2011). Origins of regulated cell-to-cell variability. Nat. Rev. Mol. Cell Biol. *12*, 119–125.

Spencer, S.L., Cappell, S.D., Tsai, F.-C., Overton, K.W., Wang, C.L., and Meyer, T. (2013). The proliferation-quiescence decision is controlled by a bifurcation in CDK2 activity at mitotic exit. Cell *155*, 369–383.

Spiller, D.G., Wood, C.D., Rand, D.A., and White, M.R.H. (2010). Measurement of single-cell dynamics. Nature *465*, 736–745.

Strasen, J., Sarma, U., Jentsch, M., Bohn, S., Sheng, C., Horbelt, D., Knaus, P., Legewie, S., and Loewer, A. (2018). Cell-specific responses to the cytokine TGFβ are determined by variability in protein levels. Mol. Syst. Biol. *14*, e7733.

Stuart, T., Butler, A., Hoffman, P., Hafemeister, C., Papalexi, E., Mauck, W.M., 3rd, Hao, Y., Stoeckius, M., Smibert, P., and Satija, R. (2019). Comprehensive Integration of Single-Cell Data. Cell *177*, 1888–1902.e21.

Sturm, O.E., Orton, R., Grindlay, J., Birtwistle, M., Vyshemirsky, V., Gilbert, D., Calder, M., Pitt, A., Kholodenko, B., and Kolch, W. (2010). The mammalian MAPK/ERK pathway exhibits properties of a negative feedback amplifier. Sci. Signal. *3*, ra90.

Tibshirani, R., Walther, G., and Hastie, T. (2001). Estimating the number of clusters in a data set via the gap statistic. J. R. Stat. Soc. Series B Stat. Methodol. *63*, 411–423.

Tirosh, I., Izar, B., Prakadan, S.M., Wadsworth, M.H., 2nd, Treacy, D., Trombetta, J.J., Rotem, A., Rodman, C., Lian, C., Murphy, G., et al. (2016). Dissecting the multicellular ecosystem of metastatic melanoma by single-cell RNA-seq. Science *352*, 189–196.

Uda, S., Saito, T.H., Kudo, T., Kokaji, T., Tsuchiya, T., Kubota, H., Komori, Y., Ozaki, Y., and Kuroda, S. (2013). Robustness and compensation of information transmission of signaling pathways. Science *341*, 558–561.

Voliotis, M., Perrett, R.M., McWilliams, C., McArdle, C.A., and Bowsher, C.G. (2014). Information transfer by leaky, heterogeneous, protein kinase signaling systems. Proc. Natl. Acad. Sci. USA *111*, E326–E333.

Ward, P.S., and Thompson, C.B. (2012). Signaling in control of cell growth and metabolism. Cold Spring Harb. Perspect. Biol. *4*, a006783.

Worster, D.T., Schmelzle, T., Solimini, N.L., Lightcap, E.S., Millard, B., Mills, G.B., Brugge, J.S., and Albeck, J.G. (2012). Akt and ERK control the proliferative response of mammary epithelial cells to the growth factors IGF-1 and EGF through the cell cycle inhibitor p57Kip2. Sci. Signal. *5*, ra19.

Yao, G., Lee, T.J., Mori, S., Nevins, J.R., and You, L. (2008). A bistable Rb-E2F switch underlies the restriction point. Nat. Cell Biol. *10*, 476–482.

Yu, G., Li, F., Qin, Y., Bo, X., Wu, Y., and Wang, S. (2010). GOSemSim: an R package for measuring semantic similarity among GO terms and gene products. Bioinformatics *26*, 976–978.

Yu, G., Wang, L.-G., Han, Y., and He, Q.-Y. (2012). clusterProfiler: an R package for comparing biological themes among gene clusters. OMICS *16*, 284–287.

Zhang, W., and Liu, H.T. (2002). MAPK signal pathways in the regulation of cell proliferation in mammalian cells. Cell Res. *12*, 9–18.

Zimmermann, S., and Moelling, K. (1999). Phosphorylation and regulation of Raf by Akt (protein kinase B). Science *286*, 1741–1744.

Zmajkovicova, K., Jesenberger, V., Catalanotti, F., Baumgartner, C., Reyes, G., and Baccarini, M. (2013). MEK1 is required for PTEN membrane recruitment, AKT regulation, and the maintenance of peripheral tolerance. Mol. Cell *50*, 43–55.

Zwang, Y., Sas-Chen, A., Drier, Y., Shay, T., Avraham, R., Lauriola, M., Shema, E., Lidor-Nili, E., Jacob-Hirsch, J., Amariglio, N., et al. (2011). Two phases of mitogenic signaling unveil roles for p53 and EGR1 in elimination of inconsistent growth signals. Mol. Cell *42*, 524–535.

STAR★METHODS

KEY RESOURCES TABLE

REAGENT or RESOURCE	SOURCE	IDENTIFIER
Antibodies		
Mouse monoclonal anti-pAKT	Thermo Fisher	Cat#MA1-20325; RRID: AB_557538
Rabbit monoclonal anti-pRB	Cell Signaling Technology	Cat#8516; RRID: AB_11178658
Rabbit monoclonal anti-pERK	Cell Signaling Technology	Cat#4370; RRID: AB_2315112
Bio-Plex Pro Human Cancer Biomarker Panel 2, EGF Set	Bio-Rad	Cat #171BC603M
Bio-Plex Protein Array system	Bio-Rad	Cat#LQ000060AK284J
Chemicals, Peptides, and Recombinant Proteins		
CHIR-98014 GSK3b inhibitor	Selleckchem	S2745; CAS:252935-94-7
Gefitinib EGFR inhibitor	Cayman Chemical	13166; CAS:184475-35-2
IKK2 inhibitor	Calbiochem	401479; CAS:354812-17-2
JNK inhibitor VIII	Cayman Chemical	Cay15946; CAS: 894804-07-0
Ly294002 PI3K inhibitor	Alexis Biochemicals	BML-ST420; CAS: 154447-36-6
MK-2206 AKT1/2/3 inhibitor	Selleckchem	S1078; CAS:1032350-13-2
Palbociclib CDK4/6 inhibitor	MedchemExpress	HY-50767; CAS: 571190-30-2
RO-3306 CDK1 inhibitor	Axon Medchem	Axon 1530; CAS: 872573-93-8
SB203580 p38 inhibitor	Selleckchem	S1076; CAS: 152121-47-6
SB216763 GSK-3 inhibitor	Sigma-Aldrich	S3442; CAS: 280744-09-4
Selumetinib (AZD6244) MEK1/2 inhibitor	Selleckchem	S1008; CAS:606143-52-6
Sorafenib RAF kinases inhibitor	Selleckchem	S7397; CAS: 284461-73-0
U0126 MEK1/2 inhibitor	Selleckchem	S1102; CAS:1173097-76-1
Hoechst 33342	Invitrogen	Cat#H3570
FluoroBrite	Thermo Fisher	Cat#A1896701
DMEM/F-12	Thermo Fisher	Cat# 21331020
HEPES	Thermo Fisher	Cat#A15630106
EGF	PeproTech	Cat#AF-100-15
IGF	PeproTech	Cat#100-11
Insulin	Sigma-Aldrich	Cat#91077C
Penicillin-Streptomycin	Thermo Fisher	Cat#15140-122
GlutaMAX	Thermo Fisher	Cat#3550-038
Cholera Toxin	Sigma-Aldrich	Cat#C8052
BSA	Thermo Fisher	Cat#11021-037
Hydrocortison	Sigma-Aldrich	Cat#H0888
Critical Commercial Assays		
EdU Click-647	Carl Roth GmbH	7777.1
Chromium Single Cell 3′ GEM, Library & Gel Bead Kit v3	10x Genomics	PN-1000075
Chromium Single Cell B Chip Kit	10x Genomics	PN-1000073
Chromium i7 Multiplex Kit	10x Genomics	PN-120262
BD Single-Cell Multiplexing Kit—Human	BD Biosciences	633781
Deposited Data		
scRNA-seq data	This study	GSE147259
Single cell time series	This study	https://dx.doi.org/10.25534/tudatalib-158
Analysis code	This study	https://dx.doi.org/10.25534/tudatalib-160
Experimental Models: Cell Lines		
Human: MCF10A FIRE	Albeck et al., 2013	NLS-mCerulean, FIRE, RFP-GMNN

(*Continued on next page*)

Continued

REAGENT or RESOURCE	SOURCE	IDENTIFIER
Software and Algorithms		
ImageJ	https://imagej.net/ImageJ	Version 1.8; RRID:SCR_003070
R	https://www.r-project.org	Version 3.6; RRID;SCR_001905
MATLAB	Mathworks	R2016b; RRID:SCR_001622
Python	https://www.python.org/	Version 3.7; RRID:SCR_008394
NIS-Elements Advanced Research	Nikon	Version 4.5; RRID:SCR_014329
Other		
Inverted fluorescence microscope	Nikon	Ti-E inverted
μ-Plate 24 Well Black	ibidi	Cat#82406

LEAD CONTACT AND MATERIALS AVAILABILITY

Lead Contact

Further information and requests for resources and reagents should be directed to and will be fulfilled by the Lead Contact, Alexander Loewer (loewer@bio.tu-darmstadt.de).

Materials Availability

This study did not generate new unique reagents.

Data and Code Availability

Time series data of all tracked cells (https://doi.org/10.25534/tudatalib-158) as well as data analysis scripts (https://doi.org/10.25534/tudatalib-160) are available online. ScRNA-seq data is available at GEO under the accession number GSE147259 (https://www.ncbi.nlm.nih.gov/geo/query/acc.cgi?acc=GSE147259). Original image data and image analysis scripts are available from the corresponding author upon reasonable request.

EXPERIMENTAL MODEL AND SUBJECT DETAILS

Cell lines

MCF10A cells were grown in DMEM/F12 medium supplemented with 5% horse serum (Thermo Fisher), 20 ng/ml EGF (PeptroTech), 0.5 μg/ml hydrocortisone, 100 ng/ml cholera toxin, 10 μg/ml insulin (all Sigma), penicillin-streptomycin and 1 × GlutaxMax^{TM} (Thermo Fisher). The FIRE reporter has been previously described (Albeck et al., 2013) . In brief, it is an indirect reporter of ERK activity, which consists of the PEST domain of FRA1 fused to YFP. Expression is driven by the MSCV LTR (murine stem cell virus long terminal repeat). The reporter cell line also stably expresses NLS-CFP (mCerulian) as a nuclear marker to facilitate automatically tracking and segmenting cells. In addition, the reporter cell line also expresses GMNN as a marker for the transition from G1- into S-phase and for division.

METHOD DETAILS

Luminex assays

We seeded 37,500 cells per well in a 24-well plate and let them grow for 48 h in complete growth medium (see above). Afterward, cells were growth factor-starved for 48 h and stimulated with either 1 ng/ml or 7.5 ng/ml EGF for different durations (0 h, 1 h, 2.5 h, 5 h and 24 h). Thirty minutes prior EGF stimulation, cells were treated with inhibitors against MEK (1 uM), GSK3 (10 uM), JNK (10 uM), p38 (1 uM), AKT (1 uM) and PI3K (50 uM). Lysates were prepared according to the supplier's protocol and analyzed with the Bio-Plex Protein Array system (Bio-Rad, Hercules, CA) using beads specific for pAKT (S473), pERK1/2 (T202/Y204, T185/Y187), pMEK1 (S217/S221), pRPS6 (S235/236), pATF2 (T71), pSTAT3 (Tyr705), pP90RSK (Ser380), pP38 (Thr180/Tyr182), p-mTOR (Ser2448), pJNK (Thr183/Tyr185), pGSK-3a/b (Ser21/Ser9) and pBAD (Ser136). For data acquisition, the Bio-Plex Manager software was used. The raw data was further analyzed using customized R-scripts.

Extracellular EGF concentrations in combination with a standard were measured in cell culture supernatants using the Bio-Plex Pro Human Cancer Biomarker 2 panel (Bio-Rad) according to the manufacturer's recommendations.

Live-cell microscopy experiments

For live-cell imaging experiments, we used 24-well imaging plates (ibidi). We seeded 37,500 cells per well and incubated them in normal medium for 36 h before a 48 h starvation period in DMEM/F12 containing 0.3% tissue culture grade BSA (Sigma),

0.5 μg/ml hydrocortisone, 100 ng/ml cholera toxin, penicillin, and streptomycin. At least 2 h before the experiment we changed medium to phenol red – free FluoroBrite medium (Thermo Fisher) containing 0.3% tissue culture grade BSA (Sigma), 0.5 μg/ml hydrocortisone, 100 ng/ml cholera toxin, 1 × glutamax, 10 mM HEPES, penicillin and streptomycin. In stimulation experiments, cells were tracked for an hour prior to EGF addition. Cells were imaged on a Nikon Ti inverted microscope enclosed with an environmental chamber controlling temperature, atmosphere (5% CO2), and humidity using a 20 × Plan Apo objective (NA 0.75) and a Nikon Qi2 camera. Cells were imaged every 20 min for up to 48 h.

EdU staining

For EdU staining in live-cell imaging, cells were incubated with 10 μM EdU (EdU Click-647) at defined time points. After 40 min, EdU was washed off with medium and the supernatant of a backup plate, which was treated equally, was utilized to ensure appropriate EGF concentrations. Immediately after the experiment, cells were fixed with 2% paraformaldehyde, washed with PBS, permeabilized with 0.1% Triton X-100/PBS and blocked with 10% goat serum/PBS. For EdU detection, a reaction cocktail was prepared according to the manufacturer's instructions and added to the cells. After 30 min incubation at room temperature, cells were washed and counterstained with 2 μg/ml Hoechst in 0.1% Triton X-100/PBS. Using the same positions, cells were imaged for one additional loop in the microscope and correlated with the previous captured images.

Immunofluorescence

Cells were seeded and treated equally to the live-cell microscopy experiments. After a 48-hour growth factor starvation, cells were stimulated with EGF at specific time points to fix all conditions with 2% paraformaldehyde simultaneously. After permeabilizing with 0.1% Triton X-100/PBS, cells were blocked with 10% goat serum/PBS and incubated with primary antibodies in 1% BSA/PBS. Washing steps using 0.1% Triton X-100/PBS and following incubation with secondary antibodies conjugated with Alexa Fluor 488 (#A-11034) and Alexa Fluor 647 (#A-21245, Thermo Fisher Scientific) in 1% BSA/PBS were performed. After further washing steps, cells were stained with 2 μg/ml Hoechst in 0.1% Triton X-100/PBS. Stored in PBS, images were acquired with a 20 × plan apo objective (NA 0.75) using appropriate filter sets. Automated segmentation was performed in MATLAB (MathWorks) with algorithms from CellProfiler (Carpenter et al., 2006).

Single cell preparation for scRNA sequencing

For scRNA sequencing, 6-cm plates were used with 4.3 × 105 cells per plate and treated equally to the live-cell microscopy experiments. After a 48-hour growth factor starvation, cells were stimulated with EGF at specific time points to trypsinize them simultaneously and adjusted the cell number to 500.000 cells per condition. Each sample was resuspended in 50 μl BD Stain Buffer (FBS) and labeled with a specific Sample Tag (10 μl) for 20 min at room temperature. After adding 100 μl BD Stain Buffer, cells were mixed, centrifuged and washed with 500 μl BD Stain Buffer. Using 500 μl RNase free PBS, all cells were pooled in a single tube and counted to ensure a sufficient cell number. After centrifugation and resuspension in RNase free PBS, pre-chilled methanol was added dropwise to the sample while mildly vortexing. Cells were kept on ice for 15 min, mixed, divided into 1 mL aliquots and stored at −80°C.

Rehydration and library preparation

Rehydration was done at 4°C; cells were pelleted and washed twice in rehydration buffer (DPBS, 10% BSA, 0.5U/μl RNase Inhibitor), then filtered and counted. The 3′ RNA library war prepared according to the "Chromium Single Cell 3′ Reagent Kits v3"-protocol (CG000183 Rev A) with a targeted cell recovery of 10.000 cells. At step 2.3.d of cDNA Cleanup the supernatant was removed and used for sample tag library preparation according to the "BD Single-Cell Multiplexing Kit—Human"-protocol (Reagent Kit v2, Doc ID: 179682 Rev. 1.0). The cDNA library was complemented with 5% of its corresponding sample tag library to be run in the same sequencing run. Samples were sequenced on an Illumina HiSeq 4000 sequencer.

QUANTIFICATION AND STATISTICAL ANALYSIS

Single cell RNA sequencing analysis

Read mapping and counting was done using cellranger version 3.0.2 using a dual genome reference consisting of the human genome GRCh38 as supplied by cell ranger, and an artificial genome containing the BD sequence tags. Demultiplexing was done using a custom script that reads the BAM file and counts sequences that map to the artificial BD sequence tags genome, and removes duplicate UMIs per cell. Subsequently, cells were assigned to samples (or duplets) using the HTODemux() function of Seurat (Stuart et al., 2019) after normalization (as described in the Seurat manual). Transcriptome analysis of the single cell RNA sequencing samples was done using Seurat (Stuart et al., 2019). In brief, low quality cells were removed based on mitochondrial contamination and number of unique genes. Each gene was normalized by the total expression in the cell, scaled by 10,000 and log-transformed. Cell cycle status was defined using a list of cell cycle markers from Tirosh et al. (2016) as provided by Seurat. For differential gene expression analysis, cells were grouped by experiment, condition, and cell cycle phase to generate pseudo-bulk samples. Differential gene expression analysis was done using DESeq2 (Love et al., 2014). To identify the effect of inhibitors on pathway activity, we used variance-stabilized data as provided by DESeq2 and applied PROGENy (Schubert et al., 2018) . The differentially expressed genes in the

pseudo-bulk samples were further analyzed using GO enrichment (R package: clusterProfiler; Yu et al., 2012). The identified GO-terms were simplified using a semantic similarity measure, which depends on the frequencies of two GO terms involved and that of their closest common ancestor term (R package: GOSemSim; Yu et al., 2010).

Data analysis of live-cell experiments

Cells were tracked throughout the duration of the experiment using custom-written MATLAB (MathWorks, Natick, MA) scripts based on code developed by the Alon lab (Cohen et al., 2008) and the Cell Profiler project (Carpenter et al., 2006) as previously described (Strasen et al., 2018). In brief, we applied flat-field correction and background subtraction to raw images before segmenting individual nuclei from images of the NLS-CFP reporter using adaptive thresholding and seeded watershed algorithms. Segmented cells were assigned to corresponding cells in subsequent images using a greedy match algorithm based on a cost function, which included the velocity and direction of movement for a cell. Additionally, the fluorescence intensity of the nuclear marker was used to ensure consistency. We then quantified the nuclear fluorescence intensity of the FIRE reporter for each cell over time and normalized the resulting single-cell trajectories by dividing with the nuclear fluorescence of the NLS-CFP reporter to account for changes in nuclear shape. This normalization eliminated spurious peaks and disturbances by cell division. The measurements of unstimulated control cells included in each experiment were used for further normalization resulting in a fold-change of FIRE levels compared to unstimulated means (Figure S1E). Specifically, for each cell the FIRE levels at each time-point were divided mean FIRE level of the unstimulated control at that time-point. Cells with an amplitude greater than three standard deviations from the average amplitude of unstimulated cells are considered to be responders.

To identify cell cycle states using Geminin, we first normalize the time courses by the mean of the unstimulated control. Time points with a Geminin response smaller than a threshold (mean + 2*sd of unstimulated control) are defined as part of the G1-phase, when Geminin is not expressed (Figure S4B). Using run-length encoding, we can identify the duration of S/G2-phase and the time point of division. To avoid false positive detection cell cycle phases, we include only cells in our analysis, where the time between beginning of S-phase and division is at least 4 h.

Percent of dividing cells was used to compare effects between different concentrations of EGF or different types of inhibitors. We calculated the standard error with bootstrapping (n = 1000, R package: boot).

Clustering

The time courses of the FIRE reporter (normalized) were clustered using Partitioning Around Medoids (PAM), which is a non-hierarchical clustering. PAM tries to partition the data by minimizing the squared error of distance measure (R package: cluster). We chose Euclidean distance, which is based on the straight-line distance between the FIRE responses at each individual time-point. In order to identify the most reasonable number of clusters, we calculated the Gap-statistic (Tibshirani et al., 2001)for an increasing number of clusters (k = 1 ... 20) (R package: cluster).

Feature analysis

The time courses were separated into early (less than 16 h after stimulation) and late response (more than 20 h after stimulation). For each signaling phase, we defined the amplitude as the mean of the three highest FIRE responses after normalization and the time of response as the mean time for the three highest FIRE responses. The fold-change is taken with respect to the mean response of FIRE in the same cell before stimulation. The $\log_2$ amplitude and the $\log_2$ fold-change were also included as features. The duration is measured as full width at half maximum, limited to the maximum possible observation period. The area under the curve has been estimated using a spline interpolation (R package: MESS). To identify responding cells, the amplitude of the first response and the second response was compared to the distribution of the respective amplitude in the control experiment (without EGF).

Information theoretical analysis

For calculating the multivariate mutual information, we grouped each feature into equidistant bins. We calculated the overlap matrix, or confusion matrix, between EGF concentrations and the different groups for each FIRE feature. A similar approach was used to define the overlap between the different groups of FIRE features and whether a cell divides (yes-or-no decision). From this we calculate mutual information, defined as

$$I(X;Y) = \sum_{x\in X}\sum_{y\in Y} p(x,y) log \frac{p(x,y)}{p(x)\cdot p(y)}$$

We bootstrapped mutual information (n = 1000, R package: boot) to ensure robustness of the calculation and report the median.

Kaplan-Meier analysis

The analysis of duration of the S/G2-phase might be affected as cells are not monitored indefinitely and thus, we have incomplete data. We are overcoming this shortcoming by calculating Kaplan-Meier curves. Kaplan-Meier curves are a way to analyze times-to-event with incomplete data. This type of analysis is commonly used in clinical studies (Bewick et al., 2004) to account for patient drop-outs. In the analysis of S/G2-phase duration, we characterize cells which go into S-phase if they undergo division (event

occurrence) in the measured time course or not (censored data). We show the cumulative events (completion of division) over time (R package: survival, survminer).

Analysis of Luminex experiment with inhibitors

First, only valid beads are included for further analysis (> 90% of the beads). The experiment was done in two replicates and the second replicate has a similar number of valid beads (> 90%) as the first one. The bead ids were mapped to the corresponding antibody names of the Luminex assay. There were 534 (465) spurious beads with 26 (26) different ids. Those beads were removed from further analysis. We bootstrapped the median (n = to calculate the amplitude and variability for each antibody. For each replicate the $\log_2$ fold-change compared to the untreated control has been calculated and the mean for the replicates is presented.

Analysis of EGF concentration

Fluorescence measurements of the EGF standard were used for a nonlinear regression (R-package: minpack.lm) of a 4-parameter logistic function:

$$FI = d + \frac{a - d}{1 + \left(\frac{EGF}{c}\right)^b}$$

The parameters of the model fit were applied to the inverse function to map fluorescence intensities of the measurements in the supernatant to EGF concentrations.